International Journal of Bifurcation and Chaos, Vol. 15, No. 11 (2005) 3509–3534
© World Scientific Publishing Company

SLOW–FAST DYNAMICS GENERATED BY NONINVERTIBLE PLANE MAPS

CHRISTIAN MIRA
19 rue d'Occitanie, 31130 Quint Fonsegrives, France
Istituto di Scienze Economiche, University of Urbino, Italy

ANDREY SHILNIKOV
Department of Mathematics and Statistics,
Georgia State University, Atlanta, GA 30303, USA

Received February 2, 2004; Revised January 3, 2005

The present paper focuses on the two time scale dynamics generated by 2D polynomial noninvertible maps T of $(Z_0 - Z_2)$ and $(Z_1 - Z_3 - Z_1)$ types. This symbolism, specific to noninvertible maps, means that the phase plane is partitioned into zones Z_k, where each point possesses the k real rank-one preimages. Of special interest here is the structure of slow and fast motion sets of such maps. The formation mechanism of a stable invariant close curve through the interaction of fast and slow dynamics, as well as its transformation into a canard are studied. A few among the plethora of chaotic attractors and chaotic transients produced by such maps are described as well.

Keywords: Noninvertible maps; canard; complex dynamics.

1. Introduction

We study the family of the following plane maps T:

$$\begin{aligned} x' &= x + G(x, y), \\ y' &= y + H(x), \quad H(x) = -\mu(x + \alpha), \end{aligned} \tag{1}$$

in which $0 < \mu \ll 1$ and $\alpha = 1 - \sigma$ are control parameters. Here, $G(x, y)$ is either a quadratic polynomial $G(x, y) = y + x^2$, or a cubic one $G(x, y) = y + dx - x^3$. Either map of the family is noninvertible, because its inverse T^{-1} may have, typically, none or two determinations (branches of inverses distinct in terms of their ranges and domains) in the quadratic case, or one or three in the cubic one. The phase plane of a noninvertible map can be divided into a number of zones Z_k, where a point has k distinct rank-one real preimages [Mira *et al.*, 1996]. So, in the quadratic case $G(x, y) = y + x^2$, where $k = 0, 2$, the map T is said to be of $(Z_0 - Z_2)$ type as its phase plane is subdivided into two unbounded regions: one, Z_2, generates two real rank-one preimages, while the other, Z_0, has no real preimage at all. In the cubic case $G(x, y) = y + dx - x^3$, k is either 1 or 3, and therefore the map T belongs to $(Z_1 - Z_3 - Z_1)$-type, meaning that (x, y)-plane is subdivided into three unbounded regions: in one of which, Z_3, a phase point has a triple of real rank-one preimages; the region Z_3 is bordered by two Z_1-type regions, where the phase point has always a single real rank-one preimage. Note that noninvertible polynomial maps are incompletely identified by their degrees. Indeed, a two-dimensional quadratic map may have Z_k-regions with the integer k equal to 2 or 4. The corresponding highest integer k may be 3, and 5, 7 or even 9 for a cubic map. So, the map's complexity depends on the highest value of k [Mira *et al.*, 1996], which is not a polynomial degree of the right-hand side of the map.

Any two such regions, Z_k and $Z_{k'}$, are separated by an arc of rank-one that is called a *critical curve LC*. It is a locus of the points in the (x, y)-plane where two branches of the inverse map

T^{-1} merge on a set, LC_{-1}, where the Jacobian of T zeroes. So, one can see that when $G(x, y) = y + x^2$, LC is a slanting line, and LC_{-1} is a vertical one. For $G(x, y) = y + dx - x^3$, the critical line LC is composed of a pair of parallel slanting lines, while LC_{-1} is made of a pair of parallel vertical ones L_{-1} and L'_{-1}.

Observe that map (1) is a slow–fast one, which is due to the smallness of μ. This implies that the rate of change of the y-variable is significantly slower than that of the fast x-variable. The development of the theory of the time-continuous singulary perturbed ODEs had begun a long time ago; its fundamentals can be found in [Mishchenko & Pontryagin, 1955; Pontryagin, 1957; Andronov *et al.*, 1959; Mishchenko & Rozov, 1975]. A system of such ODE is well known for exhibiting the relaxation oscillations where long plateaus are alternated by fast switches between the slow motion branches. This effect of two time scale dynamics is due to the presence of a small μ in front of the highest order time derivative of a phase variable. When $\mu = 0$, one can single out a slow motion manifold $\mathcal{M}_0^s$ and a complementary fast motion manifold $\mathcal{M}_0^f$ in the phase space of a slow–fast system. The attracting segment of $\mathcal{M}_0^s$ is formed by Lyapunov stable limit orbits of the fast subsystem, and the repelling part of $\mathcal{M}_0^s$ is composed of its unstable limit orbits. When $|\mu| \ll 1$, the manifold $\mathcal{M}_\mu^s$ persists, moreover it remains μ-close to its original $\mathcal{M}_0^s$ until the latter is normally hyperbolic, i.e. far from a bifurcation of a fixed point or a periodic orbit [Tikhonov, 1952; Fenichel, 1979]. An interesting dynamics may occur in some singular region of the phase space where the slow motion manifolds are no longer normally hyperbolic. An example of such behavior can be a small limit cycle bifurcating from a stable equilibrium state through the Poincare–Andronov–Hopf bifurcation. The amplitude of this cycle grows abnormally fast as a control parameter varies. Moreover, the cycle follows, in part, the unstable slow motion manifold bearing a exponential instability. This kind of orbital behavior was called a *canard* (or *French duck*) phenomenon [Callot *et al.*, 1977; Diener, 1981]. More complex discrete canards were first analyzed in [Shilnikov & Rulkov, 2003, 2004] in connection with the emergence of irregular subthreshold oscillations in slow–fast map based models of biological neurons. It is worth noticing that such discrete canards interrupted by sporadic spiking firings are shown to be due to the crossings of the stable and unstable slow motion sets (SSM and USM below), the phenomena that can only be observed near canards in periodically forced singularly perturbed plane vector fields.

Map (1) is a singularly perturbed, or slow–fast one, at values of μ small enough. The slow motion sets of the map are made up of arcs of cycles points at $\mu = 0$. The fast motion is constituted of arcs $y = c$ with c being a constant. Note that the dynamics of a slow–fast plane map may be way more complex than that of a planar ODE system, since the potential chaoticity of the former can be even enforced by the noninvertibility property of the map. Moreover, one observes that even a singular limit $\mu = 0$ in the quadratic case leads to a sequence of bifurcations that occurs while the family is moved through a *Lattes' critical case* [Lattes, 1906] related to the existence of infinitely many arcs composed of period-k ($k = 1, 2, 3, \ldots$) cycles with the multipliers $S_1 = +1$ and $S_2 = -1$. This robust complex dynamics will persist for nonzero $|\mu| \ll 1$ too. So, the analysis of the dynamics of the map $\mu = 0$ is reduced to that of the one family of one-dimensional maps $x' = x + G(x, c)$ where $y = c$ is a parameter. In some sense, the case $\mu = 0$ is "germinal" as it sets the foundation for the dynamics of the whole map at $\mu \neq 0$.

This paper is organized as follows: first we discuss some general properties of two-dimensional noninvertible maps. Section 3 focuses on some bifurcations originated by the Lattes' critical case. Sections 4 and 5 analyze the dynamics of maps of $(Z_0 - Z_2)$ and $(Z_1 - Z_3 - Z_1)$ types.

2. Behavioral Features of Noninvertible Maps

Let us consider a smooth noninvertible map T, not necessarily (1), in a plane. Any neighborhood of the critical set LC contains a point having, at least, two distinct rank-one preimages. Then, the set LC_{-1} is defined as that on which the Jacobian of the map T vanishes. One observes that the set LC satisfies the relations $T(LC_{-1}) = LC$, and $T^{-1}(LC) \supseteq LC_{-1}$. So, the iterate $LC_k = T^k(LC)$, $k = 1, 2, 3, \ldots$, constitutes the $(k + 1)$-rank critical set of the map T. In the quadratic case $G = y + x^2$, the pre-image LC_{-1} of LC is then a straight line shown in Fig. 8. In case of $G = y + dx - x^3$, it follows that LC_{-1} consists of two straight lines $= L_{-1}$ and L'_{-1}, whereas LC consist of two parallel lines L and L' , see Fig. 10 below.

A closed invariant set Ω is called *attracting* if a neighborhood U of Ω exists such that $T(U) \subset U$, and $T^n(X) \to \Omega$ as $n \to \infty$, $\forall\, X \in U$. An attracting set Ω may contain a single or several attractors, which may coexist with a repelling set. If it is so, the latter may give rise to either *chaotic transients* towards these attractors, or *fuzzy boundaries* of their basins (cf. [Gumowski & Mira, 1977; Mira, 1987; Mira *et al.*, 1996]). A *chaotic area* (d) is an invariant *absorbing area* (cf. [Mira *et al.*, 1996, p. 188]) bounded by arcs of the critical curves LC_n $(LC_0 \equiv LC)$, $n = 0, 1, 2, \ldots, p$ (where p is a finite integer or is infinite), within which computer simulations demonstrate consistently a robust chaotic behavior. Here, the term "chaotic" may be treated in a nonstrict sense, or in a strict one. Chaoticity in a nonstrict sense means that the observed dynamics reveals no regularity in numerical simulations. By chaoticity in the rigorous sense we mean that the given set (d) can be proven to be a genuine strange attractor.

Chaotic area (d) contains a fractal set Λ composed of countably many unstable cycles of various periods and with their increasing rank preimages. Let D be a basin of the attracting set (d), and ∂D be its boundary. It is shown in [Gumowski & Mira, 1978] that a contact between ∂d and ∂D is a global bifurcation that destroys (d) and gives rise to the emergence of a strange repeller SR, which is an unstable fractal set constituted by the points of Λ. As a repelling set, the strange repeller belongs to a basin boundary [Mira *et al.*, 1994, 1996].

The open set $D = \bigcup_{n\geq 0} T^{-n}(U)$ is the entire basin of Ω, i.e. D is the open set of points X whose forward trajectories converge to Ω. Its boundary ∂D is invariant for inverse T^{-1} of T, but not necessarily for T itself, defined by (1):

$$\begin{aligned} T^{-1}(D) &= D, \quad & T(D) &\subseteq D, \\ T^{-1}(\partial D) &= \partial D, \quad & T(\partial D) &\subseteq \partial D \end{aligned}$$

The strict inclusion holds iff D contains a Z_0-type region, for example, as in the quadratic case. If Ω is a connected attractor, (say, a fixed point), then the *immediate basin* D_0 of Ω is defined as the largest connected component of D containing Ω. Noninvertible maps may generate not only simply connected basins (like invertible maps), but also disconnected, or multiply connected, or both disconnected and multiply connected basins. A nonconnected (resp. multiply connected) basin D is generated from two different situations. The first one is due to the presence of a *headland* (resp. a *bay*) bounded by an arc of ∂D and an arc of the critical curve LC. In the second case, the immediate basin boundary intersects only one of the arcs of LC limiting a Z_k-region with $k \geq 3$, or the immediate basin is fully included in Z_k [Mira *et al.*, 1994, 1996].

An arc, α_0, intersecting LC_{-1} produces a fundamental interaction for its image with respect to the critical set LC as shown in [Mira *et al.*, 1996] and [Frouzakis *et al.*, 1997]. So, Fig. 1(a) represents an arc α_0 intersecting LC_{-1} at a point A_0 with some angle ϕ. If T is a smooth map, the rank-one image $\alpha_1 = T(\alpha_0)$ of this arc is a curve arc tangent (contact of order one) to LC at the point $A_1 = T(A_0)$. If T is a nonsmooth map, then LC_{-1} is a curve of the nonsmooth points of T, and hence α_1 has

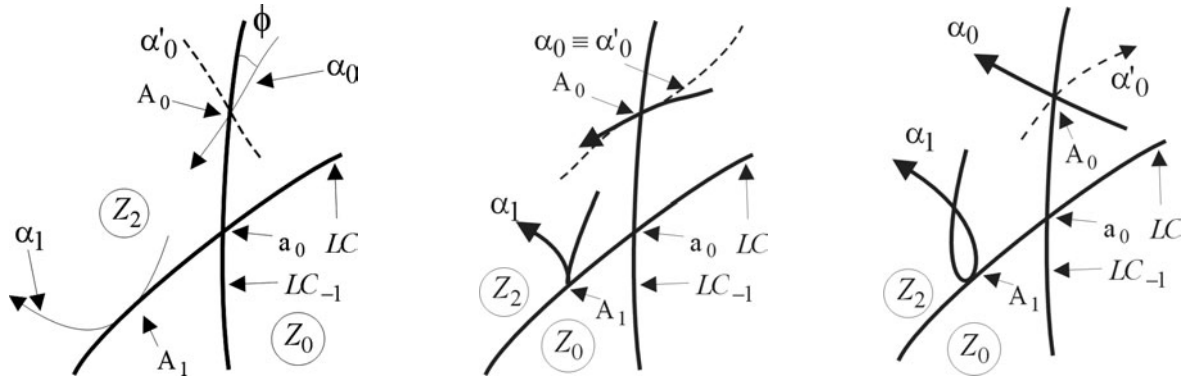

Fig. 1. Arc α_0 makes the angle ϕ at the intersection point A_0 on the curve LC_{-1} of merging rank-one preimages. Shown are three distinct contacts of rank-one image $\alpha_1 = T(\alpha_0)$ with the critical curve LC at $A_1 = T(A_0)$.

a nontransverse contact of order zero with LC. In addition to α_0, there is a second inverse α_0' of α_1 intersecting LC_{-1} at A_0. When T is smooth, one eigenvalue of the Jacobian of T along LC_{-1} remains always zero. As long as the angle ϕ stays different from the angle at the point A_0 between LC_{-1} and the eigenvector corresponding to this zero eigenvalue, the arc α_1 is quadratically tangent to LC (contact of first order at A_1).

When the arc α_0 turns, then the angle ϕ changes too. Figure 1 shows the stages of its evolution. In Fig. 1(b) the vector tangent to α_0 becomes collinear with the eigenvector corresponding to the zero eigenvalue of the Jacobian of the map at A_0. In this case, α_1 creates a cusp at A_1, so that the tangent vector to α_0' is also collinear with the null vector of the map at A_0. A further rotation leads to the first order contact of the arc with LC at A_1 [see Fig. 1(c)]; this situation differs from the former one by the local change of the parametrization direction on α_1 near A_1. This switch in the direction causes the formation of self-intersecting loops of one-dimensional unstable set of saddle orbits. The map (1) may exhibit indeed such behaviors for some parameter values. When α_0 is an arc of an invariant closed curve (γ) intersecting LC_{-1}, the situation depicted in Fig. 1(a) can only occur. Indeed, the local situation is such as one shown in Figs. 1(b) and 1(c), the existence of an arc of invariant closed curve with an irrational rotation number would mean that it would be possible to close the curve (γ) with self-intersections, or with cusps points, which makes no sense. Then, Fig. 1(b) illustrates a bifurcation turning an invariant closed curve (γ) into a "weakly chaotic ring", as established in [Mira *et al.*, 1996, pp. 529–530].

3. General Properties of Noninvertible Maps

3.1. *Some properties of invariant sets*

Functions $G(x, y)$ and $H(x)$ are introduced in (1) so that the map has always a single fixed point Q (x^*, y^*). Its stability is determined by a pair of Floquet multipliers:

$$S_{1,2} = \frac{1}{2}\left[2 + G_x^* \pm \sqrt{(G_x^*)^2 - 4\mu}\right],$$

$$G_x^* = \left.\frac{\partial G(x,y)}{\partial x}\right|_{(x^*,y^*)}$$

The point Q is a focus when $(G_x^*)^2 < 4\mu$, moreover stable provided that $G_x^* + \mu < 0$. When $G_x^* = -\mu$, Q has a pair of complex conjugate multipliers on a unit circle. This corresponds to the bifurcation of a birth of a invariant closed curve (BICC), or a torus bifurcation. The stability of the bifurcating fixed point is determined by the sign of the first Lyapunov coefficient. It is inherited later by an emerging invariant closed curve (γ), corresponding to a 2D torus in ODEs. In either, quadratic or cubic, case under consideration, the new born invariant curve is stable as follows from [Mira, 1987, p. 238], and [Arnold, 1994, p. 187].

The fixed point Q resides at the intersection of the nullclines $G = 0$ and $H = 0$. The latter ones break the (x, y)-phase plane into four subregions selected by the conditions $G > 0$, $G < 0$, $H > 0$, and $H < 0$. The images $T(G = 0)$ and $T(H = 0)$ of the nullclines cross at Q too. In the case $G = y + x^2$, $T(G = 0)$ is the parabola $y = -x^2 - \mu(x + \alpha)$, while $T(H = 0)$ is the straight line $y = x + \alpha(1 - \alpha)$. In the cubic case, $T(G = 0)$ is given by $y = x^3 - (d + \mu)x - \mu\alpha$, and $T(H = 0)$ by $y = x + (1 - d)\alpha + \alpha^3$. Because of the form of the map (1) the following assertion seems to be quite evident:

Proposition 1. *Let η be an arc of the invariant curve that intersects the nullcline $G = 0$ at a point M, its image $T(G = 0)$ at a point M', the nullcline $H = 0$ at a point N and $T(H = 0)$ at N'. Between the points M and M', there is a point where η has an infinite slope, whereas between N and N' there is a point where η has a zero slope.*

Similar to isoclines of ODEs in a plane, we can introduce and follow the qualitative evolution of the slope $m = (y' - y)/(x' - x) \equiv H/G$ of the vector $\overrightarrow{MM'}$ connecting two consecutive points: the image $M(x, y)$ and its pre-image $M'(x', y')$ at various zones of the phase plane.

3.2. *Slow and fast motion manifolds at $\mu = 0$ and $|\mu| \ll 1$*

The original map (1) at $\mu = 0$ recasts in the following form:

$$\begin{aligned} x' &= x + G(x, y), \\ y' &= y. \end{aligned} \tag{2}$$

By setting $y = c$, $c \in R^1$, the problem is reduced to the consideration of bifurcations in an one-parameter family of fast 1D noninvertible maps:

$$x' = x + G(x, c) \tag{3}$$

The dynamics of such maps, especially quadratics and cubic, were studied in [Gumowski & Mira, 1980; Mira, 1975, 1987].

When exists, the attracting set of the quadratic map (3) is composed only of a stable period-k cycle, or a chaotic segment of period-k ($k = 1, 2, 3, \ldots$). If $k > 2$, the stable cycle is associated with infinitely many sequences of unstable cycles with increasing periods, and their limit sets, that constitute a strange repeller. When the stable cycle results from a flip bifurcations sequence (period doubling) starting off the fixed point Q ($k = 2^i$, $i = 0, 1, 2, \ldots$), it coexists with a finite number of period 2^n ($n = 0, 1, 2, \ldots, j-1$) unstable cycles (absence of unstable chaos). An attracting set, if any, of the cubic map (3) with $G \equiv c + dx - x^3$ is made up of either only one stable period-k cycle, or one stable period-k chaotic segment ($k = 1, 2, 3, \ldots$), or two such attractors. If $k > 2$, they are associated with infinitely many sequences of unstable cycles, and their limit sets, with increasing period constituting one or two strange repellers.

Returning to map (1) at $\mu = 0$, let us introduce, in the phase space, the manifold SM of slow motion that is composed of all possible cycles of (3), as well as of their limit points that may exist, as c is varied. So, for example, each period-k cycle generates a set SM_k consisting of k arcs. The *stable* (resp. *unstable*) *slow dynamics manifold* SSM (resp. USM) is composed of all stable (resp. unstable) arcs SSM_k (resp. USM_k) and their limit sets. Each point on SSM_k corresponds to a period-k cycle with one (slow) multiplier S_1 equal $+1$, the other, fast, multiplier S_2 is found from the fast subsystem (3) at given $y = c$. This situation was first elaborated by Lattes [1906]:

Theorem 1 (Lattes). *Let T be a 2D analytical map generating an arc consisting of fixed points. Then, one of two multipliers, S_1 of each point equals $+1$. If the second multiplier satisfies $|S_2| < 1$, then on both sides of this arc a there is a region in the plane where the forward iterates of an initial point tend to some point of the arc, and remain on the same analytical invariant curve. When $|S_2| > 1$, an initial point starting in a small neighborhood of the arc generates a sequence of iterates running away from the arc. The same result holds for arcs of period-k cycles as well, which are the fixed points of T^k.*

Note that the more the period k increases, the more the number of period-k cycles increases as well. These cycles differ by the permutation of their points after k iterates of T. This means that a set SSM_k (resp. USM_k) is the union of arcs SSM_k^j (resp. USM_k^j) with index j characterizing the permutation; here $j = 1, 2, \ldots, p_k$, $p_k \to \infty$ if $k \to \infty$. The arcs SSM_k^j and USM_k^j, corresponding to the same permutation, join in pairs at the values of c corresponding to the fold ($S_1 = S_2 = +1$) bifurcation of the cycle defined by k and j. An arc of SSM_k^j disintegrates into two arcs belonging to $SSM_{2k}^{j'}$ after the period-k cycle undergoes a period-doubling bifurcation when $S_2 = -1$. This means for map (2) that the arcs given by ($S_1 = +1$, $|S_2| < 1$) of the stable manifold SSM of slow dynamics form an attractor, whose basin boundary contains the arcs ($S_1 = +1$, $|S_2| > 1$) of the unstable manifold USM of slow dynamics. In particular, the nullcline $G(x, y) = 0$ is the branch SM_1 of the slow dynamics manifold composed of the fixed points.

Some related bifurcations of the singularly perturbed map (1) at small $|\mu|$ are described in [Gumowski & Mira, 1980, pp. 175–177, 252–260] and in [Mira, 1987, pp. 206–211]. Their adaptation to the given problem allows the following prepositions to be made:

Let (β_k) be a set of k arcs consisting of points of a period-k cycle with the multiplier $S_1 = +1$. Depending on T^k, singular perturbations destroying (β_k) may give rise to the emergence of a period-k or a period-$2k$ cycle with $k = 1, 2, 3, \ldots$, more specifically of a fixed point $Q(-\alpha, G(-\alpha, y) = 0)$ when $k = 1$. Perturbations of the arcs existing at $\mu = 0$ generate the manifold of slow dynamics related to map (1).

The proof is given in [Gumowski & Mira, 1980] for the case $k = 1$. It is worth noting that the stable slow dynamics manifold SSM reproduces the well-known "scanning" bifurcation diagram of map (3) obtained through varying c (for example, see Fig. 2(b) below).

Let us consider an $O(\alpha^\mu)$-neighborhood ($0 < \alpha < 1$) of the nullcline $G = 0$ that narrows to $\mu \to 0^+$. Outside of $O(\mu^a)$ the following relations, characterizing the fast motion,

are hold:

$$|G(x,y)| \geq O(\mu^a),$$

$$\left|\frac{y'-y}{x'-x}\right| = |m| \leq O(\mu^{1-a}) \to 0 \quad \text{as } \mu \to 0^+.$$

A slow motion arc Ψ_r of $G=0$ is repelling if $\partial G/\partial x > 0$ in the limit $\mu \to 0^+$. A necessary condition for an arc Ψ_a of $G=0$ to attract fast motion trajectories, is $\partial G/\partial x < 0$. The repelling arc Ψ_r is comprised of unstable fixed points of the fast map with $S_2 > 1$ at $\mu = 0$. The complementary arcs $(G=0)\backslash\Psi_r$ are comprised of unstable fixed points $S_2 < -1$ at $\mu = 0$, and stable fixed points such that $-1 < S_2 < 1$.

In the cubic case where there exists a large (relaxation) stable invariant closed curve (γ), there are two arcs of fast motion, and two arcs of slow motion near both branches of Ψ_a, as illustrated in Fig. 17. The evolution of the slope $m = H/G$ of the vector $\overrightarrow{MM'}$ lets one understand better the effect of canards or French duck solutions emerging with the stable invariant closed curve right bifurcating from the fixed point. In map (1), this effect is revealed in two distinct ways. The first one brings in a small stable invariant closed curve (γ) comprised of only a single arc of fast motion and two arcs of slow motions near Ψ_r and Ψ_a, like in Fig. 15. In the second case, the duck is a large stable invariant closed curve consisting of two fast and two slow motion arcs shown in Fig. 16.

The "canard" effect implies that an arc of (γ) stays closed to the repelling arc Ψ_r of $G=0$, before the phase point on (γ) is dragged along with the fast motion towards Ψ_a. This also means that the fixed point Q, giving rise (γ), remains close enough to a fold of the graph of $G=0$, where $G_x/G_y = 0$. Note that Q is a focus when $(G_x^*)^2 < 4\mu$ at $|\mu|$ small enough, and since the bifurcation occurs when $G_x^* = -\mu$, then Q is indeed in a small neighborhood of fold $G_x^* = 0$. Hence, after the bifurcation, some arc of (γ) must remain in a neighborhood of the repelling arc Ψ_r of $G=0$.

Then, the intersection $(\gamma) \cap \Psi_r$ gives a point M on (γ) with an infinite slope between M and $M' = TM$, followed by a fast motion, an intersection $N = (\gamma) \cap \Psi_a$, an infinite slope between N and $N' = TN$, and a slow motion in the $O(\mu^a)$-neighborhood of Ψ_a. In the case $G = y + x^2$, one may see that the fast motion on (γ) is only followed by a slow motion in the Ψ_a neighborhood with a subsequent return into the Ψ_r neighborhood. It results in the appearance of a "small" invariant curve (γ). In the case $G = y + dx - x^3$, "small" invariant curve (γ) merges too. However, the fact that the nullcline $G=0$ has two extremum points may alter its evolution as a control parameter is varied in the sense that the size of (γ) may grow abnormally fast. This may also lead to the absence of an intersection between (γ) and Ψ_r. If so, when (γ) leaves a neighborhood of Ψ_r, when (γ) moves out of a neighborhood of the repelling arc Ψ_r, the fast motion pushes it toward the opposite branch of the attracting part Ψ_a of $G=0$. This leads to a sudden increase of the size of (γ) that gives rise to the so-called canard with a head. With further parameter change, the point Q moves further away from $G_x^* = 0$, resulting in shortening the length of the arc of (γ) near Ψ_r. Eventually, as no part of (γ) follows Ψ_r, the map exhibits relaxation oscillations generated by (γ) consisting of two fast motion arcs and two slow motion arcs in a neighborhood of Ψ_a.

4. $(Z_0 - Z_2)$ Map

4.1. *Basic properties*

In the case of the quadratic map T

$$\begin{aligned} x' &= x + G(x,y) \equiv x + x^2 + y, \\ y' &= y + H(x) \equiv -\mu(x+\alpha), \quad \alpha > 0, \end{aligned} \tag{4}$$

its inverse T^{-1} has two branches, or two determinations T_1^{-1} and T_2^{-1}, i.e. the jacobian of the inverse map is nullified on two loci in the (x,y)-phase plane:

T_1^{-1} :

$$\begin{cases} x = \dfrac{1}{2}(-1-\mu-\sqrt{(1+\mu)^2 - 4(y'-x'+\mu\alpha)}), \\ y = y' + \mu(x+\alpha) \end{cases},$$

T_2^{-1} :

$$\begin{cases} x = \dfrac{1}{2}(-1-\mu+\sqrt{(1+\mu)^2 - 4(y'-x'+\mu\alpha)}) \\ y = y' + \mu(x+\alpha) \end{cases}.$$

The forward map T has a single fixed point $Q(-\alpha; -\alpha^2)$ with multipliers $S_{1,2} = 1 - \alpha \pm \sqrt{\alpha^2 - \mu}$. One sees that Q is a focus, i.e. $S_{1,2}$ are complex conjugates $\alpha^2 < \mu$; moreover Q is stable if $\mu < 2\alpha$. The curve $\mu = 2\alpha$ corresponds to the BICC bifurcation after which Q becomes an unstable focus surrounded by a small stable invariant closed curve (γ), [Mira, 1987, p. 238].

The nullclines given by $G \equiv y + x^2 = 0$ and $H \equiv -\mu(x+\alpha) = 0$ divide the phase plane in four

regions where $G > 0$, $G < 0$, $H > 0$ and $H < 0$. Their images $T(G = 0)$ and $T(H = 0)$ are the parabola $y = -x^2 - \mu(x + \alpha)$, and is a straight line $y = x + \alpha(1 - \alpha)$, respectively.

4.2. *Fast dynamics at* $\mu = 0$

At $\mu = 0$, the dynamics of (4) on each leaf $y = c$ is determined by the following map:

$$x' = x^2 + x + c. \tag{5}$$

This map turns into the classical Myrberg's map $u' = u^2 - \lambda$ by letting $c = -\lambda - 1/4$ and $x = u - 1/2$. It has two fixed points: $p(c)(x = \sqrt{-c})$ which is always unstable with multiplier $S > 1$, while the other $q(c)(x = -\sqrt{-c})$ with the multiplier $S < 1$ is stable when $-1 \le c < 0$ $(-1/4 < \lambda \le 3/4)$, and is unstable (multiplier $S < -1$) for $c < -1$. Indeed the fixed points are unstable in two different ways $S > 1$ and $S < -1$, the corresponding branches having different properties. The map has a rank-one critical point $C(c - 1/4)$, which is the forward image of the minimum at $(x = -1/2)$.

The map (5) generates an attractor (stable cycle, or an attracting periodic chaotic segment) if $-9/4 < c < 0$ (or $-1/4 < \lambda < 2$ in Mybergs' notation). It is located within an absorbing segment bounded by the critical point C and its rank-one image $C_1 = T(C)$ such that $x(C_1) = c^2 + 3c/2 - 5/16$. The attractor basin is the interval

$$x(p_{-1}) < x < \sqrt{-c},$$
$$x(p_{-1}) = \frac{(-1 - \sqrt{1 - 4c + 4\sqrt{-c}})}{2},$$

where $p_{-1} = T_1^{-1}p$ is a rank-one preimage of p, other than p itself. The existence boundary of this attractor is $c_1^* = -9/4$, corresponding to $x(p) = x(C_1)$, i.e. to a homoclinic bifurcation. The classical Myrberg cascade of period-doubling occurs within the interval

$$-\frac{1}{4} < \lambda \le \lambda_{1s} \simeq 1.401155189\ldots,$$

$$\text{i.e. } c_{1s} = -\frac{1}{4} - \lambda_{1s} < c < 0.$$

This cascade creates a finite number of period-2^i cycles with $i = 0, 1, 2, 3, \ldots$. The interval

$$\lambda_{1s} \le \lambda \le 2 \quad \text{i.e. } c_1^* = -\frac{9}{4} < c < c_{1s}$$

corresponds to the generation of infinitely many sequences formed by countably many unstable cycles and their limit sets. This leads to the appearance of a strange repeller, which is a chaotic transient. As c is decreased (hence λ is increased), these cycles persist and can be then continued until $c < c_1^* = -9/4$ (i.e. $\lambda > 2$). The *snap back* repeller bifurcation of the fixed point $q(-\sqrt{-c})$ takes place at $\lambda = \lambda_{2^1}^* \simeq 1.543689013$, i.e. when $c = c_{2^1}^* \simeq -1.793689013$. Odd period cycles do not exist when $c > c_{2^1}^*$. This homoclinic bifurcation at $c_{2^1}^*$ occurs when the rank-3 critical point $C_2 = T^2(C)$ merges with the fixed point q. Similarly, other homoclinic bifurcations $c = c_{2^i}^*$ can be defined when the unstable period 2^{i-1} cycle, born through the Myrberg's cascade, merges with a rank $2^i + 1$ critical point $C_{2^i} = T^{2^i}(C)$. Moreover, the value $c = c_{1s}$ is a limit of a sequence of homoclinic bifurcation values

$$c_{2^{i+1}}^* > c_{2^i}^* > \cdots > c_{2^1}^*, \quad i = 1, 2, 3, \ldots$$
$$\text{so that} \quad c_{1s} = \lim_{i \to \infty} c_{2^i}^*.$$

When $c \le c_1^*$, there are all possible cycles and their limit sets on the x-axis, furthermore, every one is unstable. At $c = c_1^*$ these cycles and their increasing rank preimages, filling out the entire interval $[-5/2 \le x \le 3/2]$, constitute a set (E) such that the set (E') of all its limit points is perfect. The preimages of (E), are everywhere dense on (E'). When $c < c_1^*$, perturbations of (E') give rise to a *Cantor set*, made of the unstable cycles and the limit sets located within the segment $x(p_{-1}) \le x \le \sqrt{-c}$. It is now a disjoint repelling set.

When the period k increases from 3, the number of all possible period-k cycles raises very quickly. They differ by their points' permutations determined through k successive applications of the map (5). So, a period-k cycle admits the symbolism $(k; j)$, where j is an index characterizing this cyclic permutation. Moreover, the index j of a cycle of the quadratic map is the running number defining the rank of the cycle birth.

4.3. *Slow dynamics at* $\mu = 0$

Let us now consider the two-dimensional map (4) at $\mu = 0$. The manifold of slow dynamics SM is the set of all the arcs consisting of $(k; j)$-cycles $(k = 1, 2, 3, \ldots)$ with a "slow" multiplier $S_1 = +1$, and their limit set as $k \to \infty$. This set SM is composed of a stable subset SSM, where the fast multiplier $|S_2| < 1$, and of an unstable one USM, where $|S_2| > 1$.

The slow motion branch made solely of the fixed points $(k = 1)$ is given by $y = -x^2$. Its stable

segment is the arc given by $\{x < 0;\ -1 \le y < 0\}$ which is made up of stable fixed points $q(y)$ with $-1 \le S < 1$. There are two unstable arcs with $k = 1$: one consisting of unstable fixed points $p(\sqrt{-y})$ with multiplier $S_2 > 1$, located on the arc $x > 0$; the other $q(-\sqrt{-y})$ with multiplier $S_2 < -1$ is located on the slow motion arc given by $\{x < 0;\ y < -1\}$. The other branches of the slow dynamics manifold are obtained from the fractal bifurcation structure of box-within-a-box (or embedded boxes) [Mira, 1975, 1987; Guckenheimer, 1980] type of the interval $-9/4 \le y = c < 0$, and from the situation with $y < -9/4$ described above (existence of the real set (E)).

The basin of the attractor SSM is inside an open domain U bounded by four arcs: the unstable slow dynamics one $y = -x^2$ $(x > 0)$, the arc

$$\left\{(\eta) : x = \frac{(-1 - \sqrt{1 - 4y + 4\sqrt{-y}})}{2}\right\}$$

(i.e. the other rank-one preimage of $y = -x^2$, $x > 0$), the horizontal segment $(y = 0;\ -1 < x < 0)$, and the horizontal segment $\Delta : (y = -9/4,\ -5/2 < x < 3/2)$. This domain U contains a subset of the unstable manifold USM, and thus it is not the basin D of the attractor SSM. Remind that USM is the union of arcs USM_k^j $(k = 1, 3, 4, \ldots.)$ of unstable $(k; j)$-cycles, their increasing rank preimages, and the limit of all these sets. This situation leads to a fractal unstable manifold of slow dynamics. So, the boundary ∂D of the basin D is complex. It consists of two parts. The first one, USM_i, is located inside U, and gives rise to a chaotic transient toward SSM. The other part USM_o is located outside of U, and originates from the fractal perfect set (E') on Δ. It becomes completely disjoint, turning into a Cantor set of arcs in $y < -9/4$. In particular, ∂D contains the increasing rank preimages of the arc $(\tilde{\eta}) = (\eta) \cap (y < -9/4)$, i.e. $\bigcup_{n\ge 0} T^{-n}(\tilde{\eta}) \in \partial D$ (located inside the Z_2 region). When $n \to \infty$, the limit of $T^{-n}(\tilde{\eta})$ is the set of the repelling cycle arcs in the region $y < -9/4$, their limit when the period tends toward infinity, and their increasing rank preimages. It is worth noting that $\partial D \supset USM$ is invariant for T^{-1}, not for T, due to the presence of a Z_0 region containing the arc $(\eta) \cap (-9/4 < y < 0)$.

Figure 2(a) shows the region U and the rank-r preimages $(r = 1, 2)$ of the arc $(\tilde{\eta})$. The rank-one preimage $(\tilde{\eta})_{-1} = T^{-1}(\tilde{\eta})$ is formed by two branches

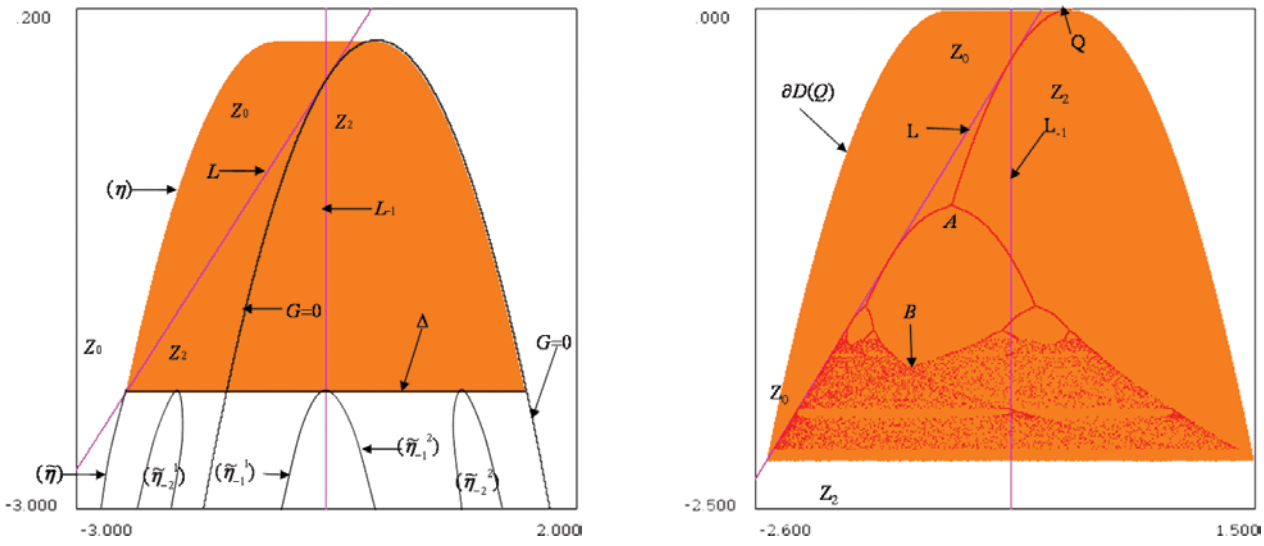

(a) (b)

Fig. 2. (a) Map (4) at $\mu = 0$, $\alpha = 0.003$. Shown are the U-region (orange) and the rank-r preimages $(r = 1, 2)$ of the arc $(\tilde{\eta})$; L is the critical curve, L_{-1} is the line of rank-one merging preimages. (b) Map (4) at $\mu = 0.0001$, $\alpha = 0.003$. Stable manifold SSM of the slow dynamics associated with the stable fixed point $Q(-\alpha; -\alpha^2)$, emerges from the bifurcation of the arc $[y = -x^2] \cap (-1 < x < 0)$ of stable fixed point q at $\mu = 0$. The manifold SSM corresponds to the red arcs, transient toward Q from the initial point $(x = 1.4,\ y = -2.2)$. The classical bifurcation diagram of an unimodal map can be recognized. The basin has infinitely many narrow tongues in the region $y < -9/8$, which is not seen at the figure scale.

of a parabolic shape $(\tilde{\eta}_{-1}) = (\tilde{\eta}^1_{-1}) \cup (\tilde{\eta}^2_{-1})$ and $(\tilde{\eta}^1_{-1}) = T_1^{-1}(\tilde{\eta})$, $(\tilde{\eta}^2_{-1}) = T_2^{-1}(\tilde{\eta})$ tangent to the line $y = -9/4$ at the point $C_{-1}(x = -1/2)$. The rank-two preimage is composed of two arcs with a maximum on $y = -9/4$, $(\tilde{\eta}^1_{-2}) = T_1^{-1}(\tilde{\eta}_{-1})$, $(\tilde{\eta}^2_{-2}) = T_2^{-1}(\tilde{\eta}_{-1})$. The set $\bigcup_{n\geq 0} T^{-n}(\tilde{\eta})$ is an arborescent sequence of parabolic shaped arcs with a maximum on $y = -9/4$, the rank-n preimage $T^{-n}(\tilde{\eta})$ consisting of 2^{n-1} such arcs. The set $[\bigcup_{n\geq 0} T^{-n}(\tilde{\eta})] \cap (y = c)$, $c < -9/4$ is a Cantor one.

4.4. *Behavior at* $0 < \mu \ll 1$

At these values of μ, the slow dynamics manifold inherits the dynamics and the bifurcations of the robust Lattes' critical case ($S_1 = +1$) are discussed above. Suppose that the parameter values are chosen so that the map has an attractor. Then, the stable manifold SSM of the slow dynamics associated with this attractor can be easily visualized. It can be as shown in Fig. 2(b) at $\mu = 0.0001$ and $\alpha = 0.003$; these values correspond to the existence of a stable fixed point $Q(-\alpha; -\alpha^2)$ born through the bifurcation of the arc $[y = -x^2] \cap (-1 < x < 0)$ of stable fixed points q at $\mu = 0$. So, SSM, shown by the red arcs, reproduces the well-known bifurcation diagram of a one-dimensional unimodal map obtained via the parameter scanning. When $\mu = 0$, the point A marks the period-doubling bifurcation of the fixed point q (at $\lambda = 3/4$, i.e. when $y = -1$), and B marks the snap back repeller bifurcation occurring at $c = c^*_{2^1}$. The part of the unstable manifold USM_i of the slow dynamics inside the region U is composed of infinitely many arcs filling in the space between SSM arcs. Figure 2(b) shows also that the stable manifold SSM has contacts with the critical line L. In this figure the orange area corresponds to the basin $D(Q)$ of the stable fixed point Q; its boundary is labeled as $\partial D(Q)$. At the given figure's scale one may see that the lowest part of the basin appears to be bounded by $y \simeq -9/8$, which is not true. Indeed the unstable manifold USM of slow dynamics, originating through the bifurcation of the USM arcs defined at $\mu = 0$, continues for $y < -9/8$ (a part of USM_0) and leaves the domain U. Therefore, the basin has infinitely many narrow tongues in the region $y < -9/8$. A section $y = c$ gives a Cantor set of disjoint points, which limit infinitely many open segments belonging to the basin $D(Q)$.

The form of the boundary $\partial D(Q)$ can be better seen when μ is increased like in Fig. 3(a). The fixed point Q is now an unstable focus surrounded by a stable invariant closed curve (γ). The arcs $(\tilde{\eta})_{-1}$, $(\tilde{\eta}^1_{-2})$ and $(\tilde{\eta}^2_{-2})$, found at $\mu = 0$, have turned into the arcs $(\tilde{\eta}_{-1})_\mu$, $(\tilde{\eta}^1_{-2})_\mu$ and $(\tilde{\eta}^2_{-2})_\mu$, respectively.

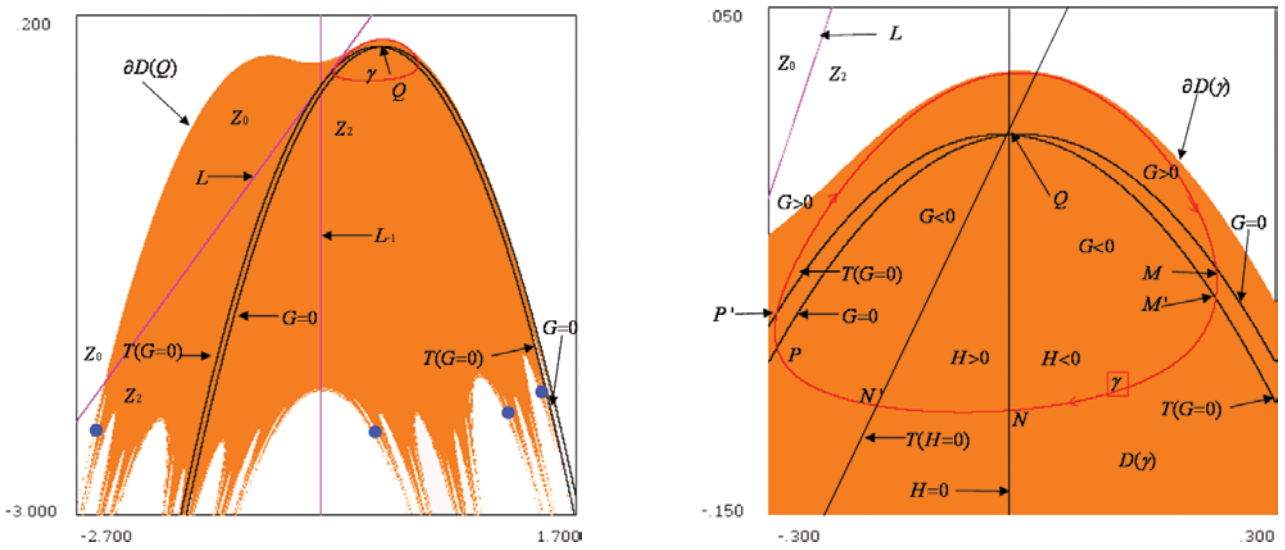

(a) (b)

Fig. 3. (a) Map (4) at $\mu = 0.1$, $\alpha = 0.03$. The fixed point Q is now an unstable focus surrounded by a stable invariant closed curve (γ) (red). An unstable period-four cycle, generated by bifurcation of a period-four arc USM_k is marked by four blue points. (b) Map (4) at $\mu = 0.05$, $\alpha = 0.015$. The fixed point Q is an unstable focus surrounded by a stable invariant closed curve (γ). A slow motion arc of (γ) follows the repelling arc of $G = 0$. It does not cross L_{-1}, and thus has no contact with L either.

This figure shows that the basin boundary $\partial D(\gamma)$ has common points with $y = -\infty$. The Lattés' bifurcation of a period-k arc USM_k^j (existing at $\mu = 0$, cf. Sec. 3.2) outside of the domain U, generates an unstable period-k cycle. Figure 3(a) reveals one of such cycle of period four with multipliers $S_1 = 1.1391$ and $S_2 = -42.08$. This cycle does not come from a period-doubling bifurcation of the period-two cycle. Another unstable period-three cycle belonging to $\partial D(Q)$ has multipliers $S_1 = 1.0254$, $S_2 = -102.36$ (the coordinates of one of its points are $x \simeq 2.15691$, $y = -5.65758$, because when $y < -3$ it is located outside the figure frame). All the cycles issued from the Lattés' bifurcation of the arcs USM_k^j, outside of the domain U defined for $\mu = 0$, are located on the part of the boundary $\partial D(Q)$, which limits the infinitely many "tongues" of the figure (attaining $y = -\infty$).

4.5. *Stable invariant sets*

4.5.1. *Invariant close curve in the invertible case situation*

A stable invariant close curve (γ) with basin $D(\gamma)$ originates from the fixed point $Q(-\alpha; -\alpha^2)$ when $(\mu = 2\alpha)$. This point is a stable focus when $\mu < 2\alpha$ and $\alpha^2 < \mu$. It turns into an unstable focus surrounded by (γ) when $\mu > 2\alpha$. One can see that since Q is in a $O(\mu)$ neighborhood of the maximum $(0; 0)$ of the nullcline $G = 0$ when $\mu > 2\alpha$ and $\mu \simeq 2\alpha$ small enough, then an arc of (γ) has to remain in a $O(\mu^a)$ $(0 < a < 1\ )$ neighborhood of the repelling arc Ψ_r given $(y = -x^2) \cap (x > 0)$ of $G = 0$. This condition is a single possibility for the existence of a "small" invariant closed curve in a $Z_0 - Z_2$ map (4) illustrated in Fig. 3(b), which is intended to show the evolution of the vector joining two consecutive points (x, y) and (x', y'). Note that (γ) cannot cross $\partial D(\gamma)$. It is suggested by the $\partial D(\gamma)$ shape and the evolution of the slope $m = (y' - y)/(x' - x)$ that a slow motion arc of (γ) remains near the repelling arc of the nullcline $G = 0$. Let us begin from the highest point on (γ) moving clockwise. This occurs when the negative slope of a tangent to (γ) is decreasing up to the point $M \in (\gamma) \cap (G = 0)$, thereby implying a vertical tangency between M and $M' \in T(G = 0)$. Between the points N and N' the fast motion arc of (γ) has an horizontal tangency. Beginning with the point P, a part of (γ) remains $O(\mu^a)$-close to the attracting arc of $G = 0$, and then has a vertical tangency between P and P'.

The second inverse T_2^{-1} of the map T near the invariant close curve (γ) can be viewed as an invertible map, provided that (γ) does not cross the line of coincident preimages L_{-1} and has no contact with the critical line L either. This situation is represented in Fig. 3(b) for $\mu = 0.05$ and $\alpha = 0.015$. Fixing $\mu = 0.01$ and decreasing α from $\alpha = 0.00252$ reveals that the invariant curve (γ) behaves as it should in a plain invertible map, until its gets destructed after contact with its basin boundary $\partial D(\gamma)$ at $(\alpha \simeq \alpha^* = 0.0025)$. Note that (γ) grows rapidly as α is increased, i.e. it is highly sensitive to small variations of the control parameter. About $\alpha = \alpha^* + 3.810^{-16}$, (γ) appears to have turned into a weakly chaotic ring $(\tilde{\gamma})$ [see Fig. 4(a)] with its basin boundary $\partial D(\tilde{\gamma})$ looking rather "fuzzy", as shown in Fig. 4(b). The exact numeric value of corresponding α is hardly determinable here, due to unavoidable round-ups and truncation errors caused by the specific computer arithmetic. Furthermore, a different computer platform would probably give different quantities like in the case of rigid basins. Therefore, we have to rely only upon a qualitative interpretation of the results. Note that the effect depicted in Fig. 4 can be a purely numerical artefact as well, or this announces an homoclinic situation where the attractor breaks down via a heteroclinic tangency.

4.5.2. *Noninvertibility for attractor and its basin*

Scarcely has the stable close invariant curve (γ) crossed the merging preimages line L_{-1} at points $P = (\gamma) \cap L_{-1}$ and $P' = T(P) \in L$, its behavior changes drastically leading to the emergence of "oscillations" on (γ), see Figs. 1 and 5(a). The further decreasing α at fixed $\mu = 0.23$ leads to bifurcation sequences described in [Mira *et al.*, 1986, pp. 515–547]. These sequences are characterized by alternation of α intervals corresponding to period-k cycles pair "saddle-node (or focus)", and intervals related to the existence of a weakly chaotic ring. Figures 5(b) shows such a weakly chaotic ring $(\tilde{\gamma})$ at $\alpha = 0.05811$. Further decreasing α gives rise to a chaotic area (d), shown in Figs. 6(a) and 6(b). Observe that the basin $D(d)$ is multiply connected, even though this cannot be seen at the figure scale. When $\mu = 0.05$, the attractor gets destroyed at $\alpha_b \simeq \alpha^* = 0.0125$, after contact with its basin

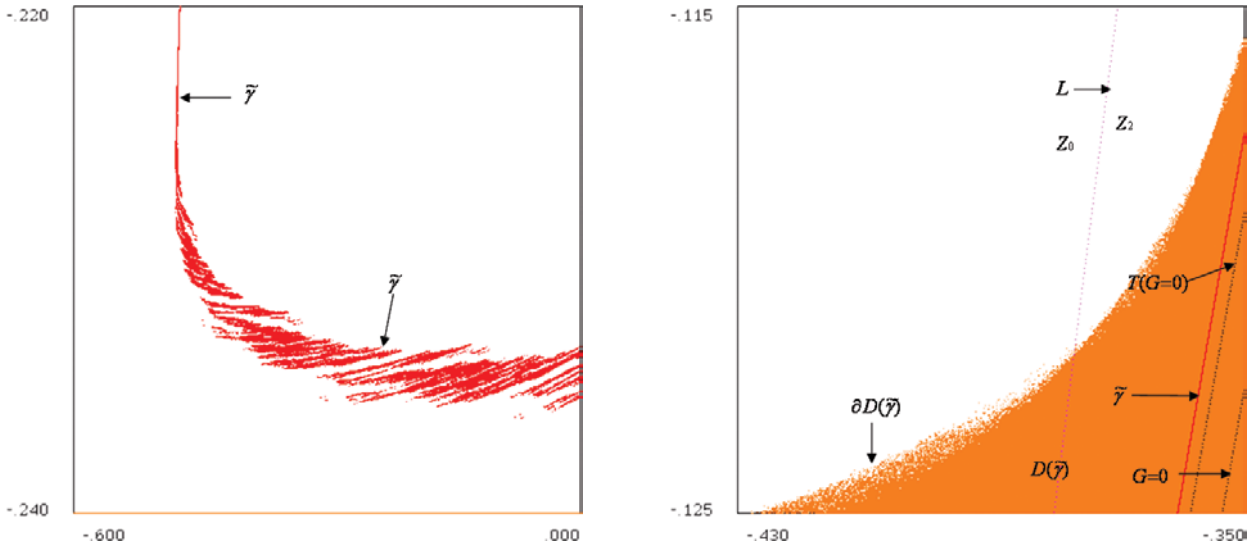

(a) (b)

Fig. 4. (a) Attractor of (4) at $\mu = 0.01$ and $\alpha = 0.0025 + 3.8\,10^{-16}$ breaks down when it contacts its own basin boundary. View of the attractor in its fast motion. (b) The basin boundary becomes "fuzzy" near the slow motion arc.

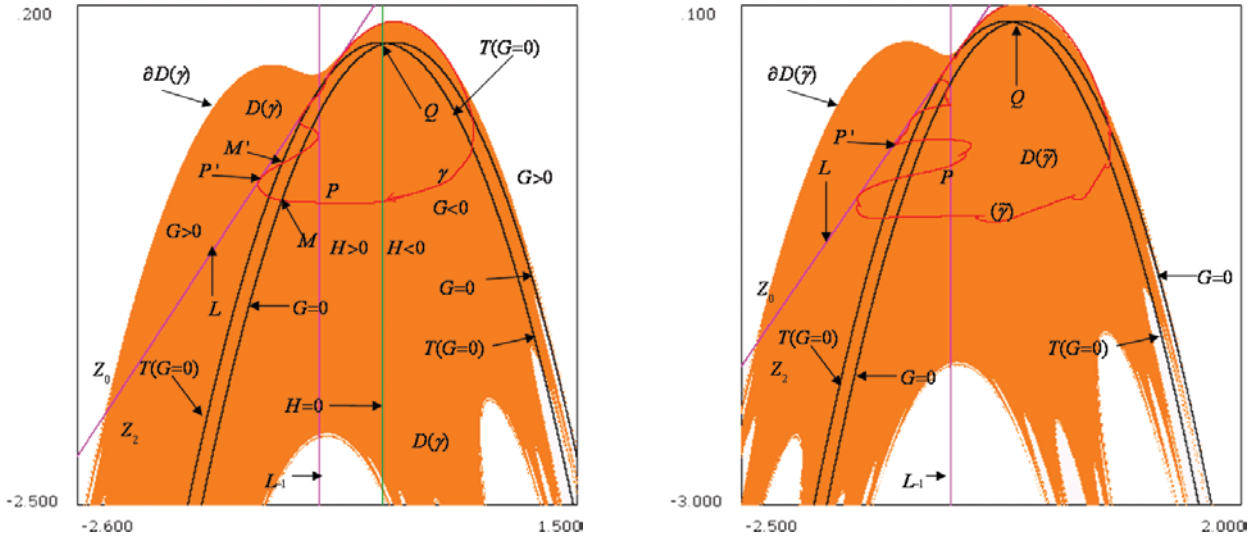

(a) (b)

Fig. 5. (a) Map (4) at $\mu = 0.23$ and $\alpha = 0.6$. While crossing L_{-1}, the stable invariant closed curve (γ) is tangent to the critical line L; this creates oscillations along L. (b) Map (4) at $\mu = 0.23$ and $\alpha = 0.05811$ shows a weakly chaotic ring $(\tilde{\gamma})$; compare with Fig. 1(b).

boundary. Staring from $\alpha = 0.01251$, there exists a stable invariant close curve (γ). As α is decreased, (γ) grows very quickly and starts oscillating transforming into weakly chaotic ring $(\tilde{\gamma})$. Moreover the attractor basin becomes multiply connected in accordable with the description reported in [Mira *et al.*, 1994, 1996].

Figure 7(a) at $\alpha = \alpha^* + 2.8\,10^{-15}$ illustrates such situation, which is due to the emergence of bay H_0 whose increasing rank preimages create two sequences of lakes (white holes belonging to the domain of diverging orbits) with unstable fixed point Q and its preimage Q_{-1} as their limit points. The enlargements in Figs. 8(a) and 8(b) allow one

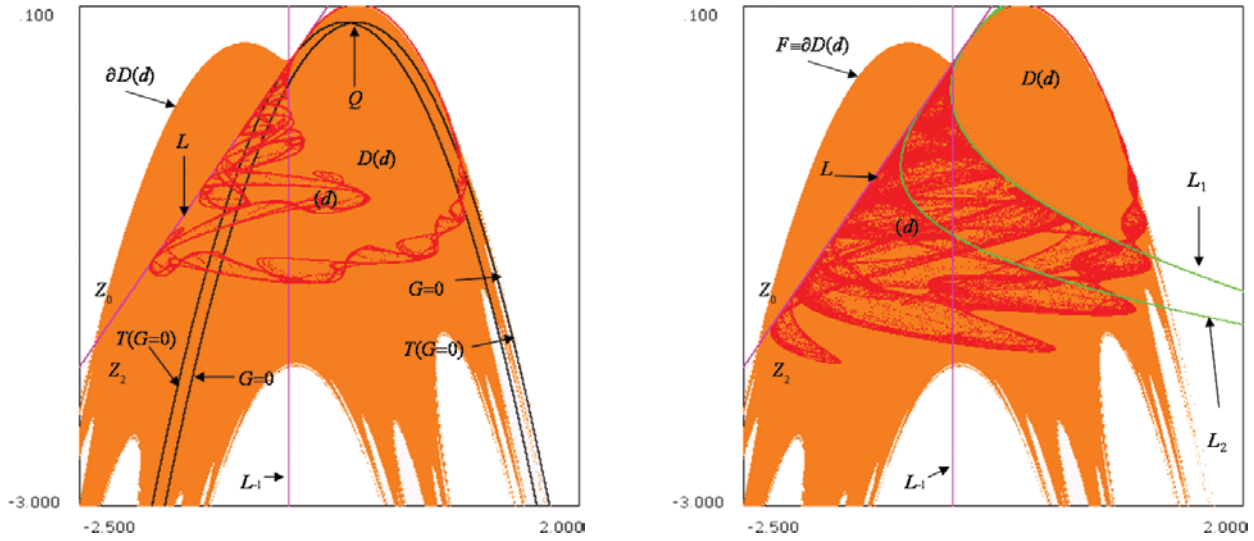

(a) (b)

Fig. 6. (a) Map (4) at $\mu = 0.23$ and $\alpha = 0.0577$. Decreasing α gives rise to the emergence of a chaotic area (d) when its basin $D(d)$ becomes multiply connected (not seen at the figure scale). (b) Chaotic area (d) of map (4) at $\mu = 0.23$ and $\alpha = 0.05758$. The crucial part of the slow motion remains in a neighborhood of the basin boundary. The basin $D(d)$ is multiply connected.

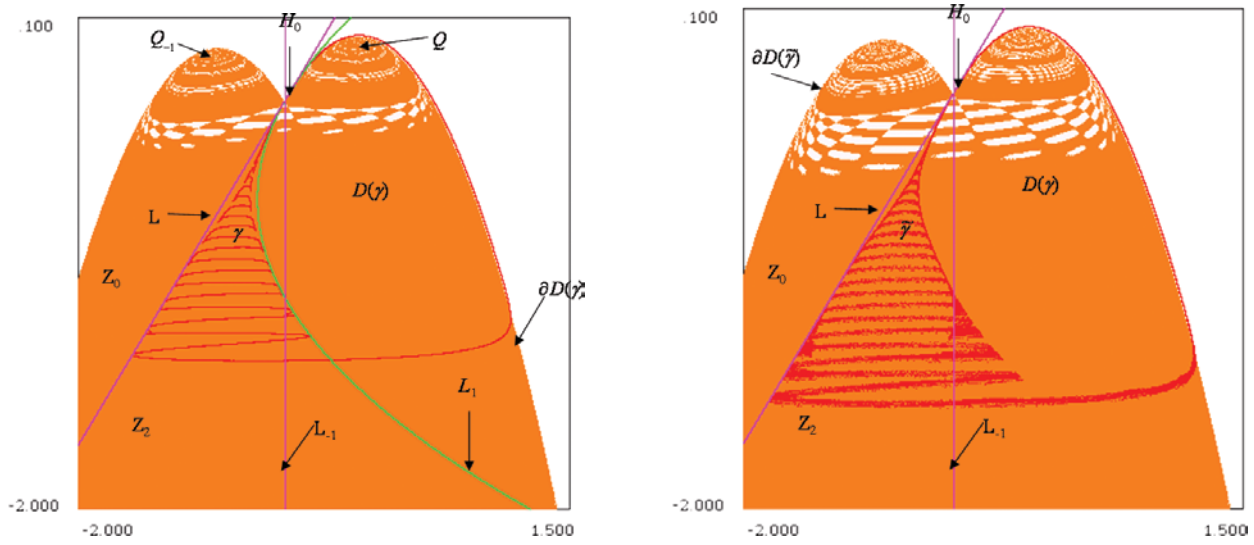

(a) (b)

Fig. 7. (a) Map (4) at $\mu = 0.23$ and $\alpha = 0.0125 + 2.8\,10^{-15}$. The points $(\gamma) \cap L_{-1}$ give rise to tangential contacts of (γ) with L evolving into oscillations on (γ). The bay H_0 has infinitely many increasing rank preimages; each generates two sequences of *lakes* having Q and its preimage Q_{-1} as limit points. Figures 12 and 13 show a high sensitivity with respect to very small variations of α. (b) Map (4) at $\mu = 0.23$, $\alpha = 0.0125 + 10^{-16}$ produces the closed curve (γ) turning into a weakly chaotic ring $(\tilde{\gamma})$.

to see the rank-one and -two lakes $H_1 = T^{-1}(H_0)$ and $H_2^1 \cup H_2^2 = T^{-1}(H_1)$. The other lakes belong to the set $\bigcup_{n>0} T^{-n}(H_0)$. It is interesting to note that the lakes sequence is made up of lakes subsets organized along "mean lines" of fast motion and "mean lines" of slow motion.

Figure 7(b) shows the stable closed curve (γ) turning into a weakly chaotic ring $(\tilde{\gamma})$ and its multiply connected basin at $\alpha = \alpha^* + 10^{-16}$. The ring has an arc that follows closely the basin boundary, which is an element of the unstable manifold of slow motion. The parameter value α is very

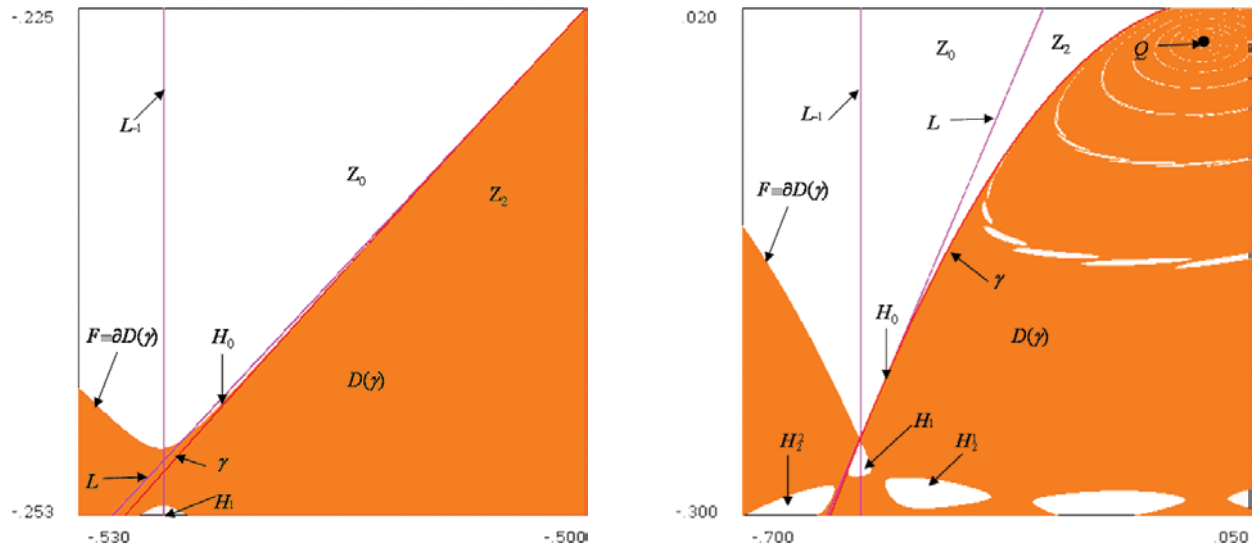

(a) (b)

Fig. 8. Map (4) at $\mu = 0.23$ and $\alpha = 0.0125 + 2.8\,10^{-15}$. Enlargements of Fig. 11 permits to see the rank-one and -two lakes $H_1 = T^{-1}(H_0)$, $H_2^1 \cup H_2^2 = T^{-1}(H_1)$. The other lakes belong to the set $\bigcup_{n>0} T^{-n}(H_0)$. The lake sequences follow subsets of fast motion, and subsets of low motion.

close to the bifurcation destroying $(\tilde{\gamma})$. As above, the presented numerical results indicate the problem of unavoidable presence of roundups and truncation errors generated by the computer, which are associated with its arithmetic. These results must be considered as qualitative, as trajectory behavior becomes extremely sensitive to small variations of the parameter α.

5. $(Z_1 - Z_3 - Z_1)$ Map

5.1. *Basic properties*

Such a cubic map T is given by:

$$\begin{aligned} x' &= x + y + dx - x^3, \\ y' &= y - \mu(x + \alpha), \end{aligned} \tag{6}$$

with $\alpha = 1 - \sigma$, $d > 0$ and $0 < \mu \ll 1$. The equation of the line $LC_{-1} = L_{-1} \cup L'_{-1}$ of merging preimages is given by:

$$x = \pm\sqrt{\frac{1 + \mu + d}{3}},$$

and that of the critical curve $LC = L \cup L'$ is given by

$$y = x \mp \left(\frac{2}{3}\right)(1 + \mu + d)\sqrt{\frac{1 + \mu + d}{3}} - \mu\alpha.$$

The inverse map T^{-1} has one or three determinations, which are the real solutions of the cubic equation:

$$x^3 - (d + 1 - \mu)x + x' + y' + \mu\alpha = 0,$$

with $y = y' + \mu(x + \alpha)$. There is a single point $Q(-\alpha; \alpha(\alpha^2 - d))$ at a finite distance from the origin. Its multipliers are

$$S_{1,2} = \frac{2 + d - 3\alpha^2 \pm \sqrt{\Delta}}{2},$$
$$\Delta = (d - 3\alpha^2)^2 - 4\mu.$$

The fixed point Q is a focus when $\mu > (d - 3\alpha^2)^2/4$; moreover it is stable if $\mu + d < 3\alpha^2$. The parameter values $\mu + d = 3\alpha^2$ correspond to the BICC bifurcation after which Q becomes unstable surrounded by a stable invariant closed curve (γ).

The nullclines $G \equiv y + dx - x^3 = 0$ and $H \equiv -\mu(x + \alpha) = 0$, divide the phase plane in four regions when $G > 0$, $G < 0$, and $H > 0$, $H < 0$. Likewise $Z_0 - Z_2$ map, these curves and their images $T(G = 0)$, $T(H = 0)$ help us give a qualitative geometrical interpretation of the behavior of deviations $x' - x$ and $y' - y$. The set $T(G = 0)$ is the cubic parabola $y = x^3 - (d + \mu)x - \mu\alpha)$, whereas $T(H = 0)$ is the straight line $y = x + (1 - d)\alpha + \alpha^3$.

5.2. *Fast dynamics at* $\mu = 0$

At $\mu = 0$ the fast dynamics is defined on each cut on $y = c$ by the one-dimensional map T'

$$x' = (d+1)x - x^3 + c \tag{7}$$

This map has two rank-one critical points

$$x(C) = c + \left(\frac{2(d+1)}{3}\right)\sqrt{\frac{d+1}{3}},$$

$$x(C') = c - \left(\frac{2(d+1)}{3}\right)\sqrt{\frac{d+1}{3}}.$$

Every bounded limit orbit, if any, is located inside the interval bounded by the points (ζ_1, ζ_2) of an unstable period-two cycle with multiplier $S > 1$. The limits of the existence region of such an orbit are determined by the two homoclinic bifurcations $x(C) = x(\zeta_2)$ at $c = c_1^*$, and $x(C') = x(\zeta_1)$ at $c = c_1'^*$; the existence interval of an attracting set is $c_1'^* < c < c_1^*$. Letting $T'^{-1}(\zeta_{1,2}) = T'(\zeta_{1,2})$, and $\overline{\Delta} = (\zeta_{1,2} - c)^2/4 - (d+1)^3/27$, the coordinates $\zeta_{1,2}$ are defined through the following relationship:

$$\sqrt[3]{\frac{d+1}{2} + \sqrt{\overline{\Delta}}} + \sqrt[3]{\frac{d+1}{2} - \sqrt{\overline{\Delta}}} = (d+1)\zeta_{1,2} - \zeta_{1,2}^3 + c. \tag{8}$$

The inverse map T'^{-1} has two coincident preimages at $c = c_1^*$ and $c = c_1'^*$ satisfying

$$\zeta_{1,2} = \frac{27c \pm 2\sqrt{27(d+1)^3}}{27}$$
$$0 = 27(\zeta_{1,2} - c)^2 - 4(d+1)^3. \tag{9}$$

The bifurcations of (7) at $c = 0$ are described in [Gumowski & Mira, 1980, pp. 415–418]. Within the interval $0 \le d \le \sqrt{27}/2 - 1$, two attractors of the map may coexist, one is located on the ray $x < 0$, and the other is on the opposite side. As the parameter d is varied, both give rise a fractal bifurcation structure of embedded boxes mentioned in Sec. 3.2. Within $\sqrt{27}/2 - 1 \le d \le 2$, some new, even period cycles, symmetric about the origin, are created, in addition to pairs of odd period cycles. On the leaf $c = 0$, the abscissa $x(\zeta_{1,2})$ is given $y = \pm\sqrt{2+d}$, and the map has all the possible cycles at $d = d_1^* = 2$. When $c \neq 0$, the map becomes dissymmetric and hence may have only one attractor.

On leafs $c = c_1^*$ and $c = c_1'^*$ the map has all the possible cycles and their limit sets in the x-axis; moreover, all of them are unstable. These cycles and their increasing rank preimages constitute a real set (E), filling out the whole interval bounded by the points ζ_1 and ζ_2. The set (E') of all the limit points of (E) is a perfect one. The preimages of (E) are dense everywhere on (E'). When $c < c_1'^*$ and $c > c_1^*$, unstable cycles and the limit sets form a Cantor set, a disjoint repelling set resulting from a perturbation of (E').

5.3. *Slow dynamics at* $\mu = 0$

Let us next examine the two-dimensional map (2) at $\mu = 0$. The manifold SM of slow dynamics consists of the arcs formed by all period-k cycles $(k = 1, 2, 3, \ldots)$ and by their limit set as $k \to \infty$. This manifold can be decomposed into the stable subset SSM $(|S_2| < 1)$ and unstable one USM $(|S_2| > 1)$. The branch SM_1 $(G = 0)$ of slow dynamics corresponding to the single fixed point $(k = 1)$ is given by $y = x^3 - dx$. Its unstable part USM_1 is made up of three parts. One arc Ψ_r made up of unstable fixed points with multipliers $S_1 = 1$ and $S_2 > 1$, is located between the two extrema $(-\sqrt{d/3} < x < \sqrt{d/3})$ of $y = x^3 - dx$. The two other arcs Ψ_r^i, $i = 1, 2$ are made up of unstable fixed points with multipliers $S_1 = 1$ and $S_2 < -1$. On curve $y = x^3 - dx$ they are defined by the inequalities $y < -[2(1-d)\sqrt{(2+d)}]/\sqrt{27}$ and $y > [2(1-d)\sqrt{(2+d)}]/\sqrt{27}$, or $x < -\sqrt{(2+d)/3}$ and $x > (2+d)/3$. The stable part SSM_1 of SM_1 is made up of two arcs Ψ_a^i $(i = 1, 2)$ of stable fixed points $q(c)$, whose multipliers satisfy $S_1 = 1$ and $-1 \le S_2 \le 1$. On the curve $y = x^3 - dx$ they are defined by the inequalities $-\sqrt{(2+d)/3} < x < -\sqrt{d/3}$ and $\sqrt{(2+d)/3} > x > \sqrt{d/3}$. Let us denote by Ψ_a^1 the arc $x < 0$ and by Ψ_a^2 the arc $x > 0$. The other branches SM_k^j $(k > 2)$ of the slow dynamics manifold are obtained from the fractal bifurcation structure of *embedded boxes* of the interval $c_1'^* \le y = c \le c_1^*$.

Figure 9 represents the basin D (shown in orange) of the attractor SSM formed by the arcs of stable period-k cycles with multipliers $S_1 = 1$, $|S_2| < 1$ at $\alpha = -0.4$ and $d = 0.65$. It is located inside an open domain (W) of nondiverging orbits bounded by two arcs $\widehat{U'V'}$, and $\widehat{UV}$ of unstable period-two cycles, and two horizontal segments $\overline{U'U}$ and $\overline{V'V}$. These arcs $\widehat{U'V'}$ and $\widehat{UV}$ belong to the two branches (η) and (η') of (8) comprised of the points (ζ_1) and (ζ_2) of unstable period-two cycles. The ordinates U, V, U', V' are such that $y(V', V) = c_1'^*$, $y(U', U) = c_1^*$, as defined in (9). The abscissae

$x(V',V)$, $x(U',U)$ are also given by (9). The open domain (W) contains a subset USM_i of the unstable manifold USM, and thus (W) is not the basin D of the attractor SSM. The boundary ∂D of the basin D is complex and includes the fractal unstable manifold USM of slow dynamics constituting a strange repeller. This boundary ∂D has a part USM_i giving rise to a chaotic transient toward SSM, and a part USM_o outside of (W) issued from the fractal perfect set (E') on $\overline{U'U}$, $\overline{V'V}$. This set becomes completely disjoint having turned into a Cantor set when in $y < c_1'^*$ and $y > c_1^*$. In particular, ∂D contains the increasing rank preimages of the arcs

$$(\tilde\eta) = (\eta) \cap (y > c_1^*), \quad (\tilde\eta') = (\eta') \cap (y < c_1'^*),$$

i.e. $\bigcup_{n\geq 0}[T^{-n}(\tilde\eta) \cup T^{-n}(\tilde\eta')] \in \partial D$. When $n \to \infty$, the limit of $T^{-n}(\tilde\eta) \cup T^{-n}(\tilde\eta')$ is the set of repelling cycle arcs in the regions $y < c_1'^*$ and $y > c_1^*$.

Figure 9 shows the region (W) and the rank-one preimages of the arcs $(\tilde\eta)$, as well as $(\tilde\eta')$. The rank-one preimage $(\tilde\eta)_{-1} = T^{-1}(\tilde\eta)$ is constituted by two branches $(\tilde\eta_{-1}) = (\tilde\eta^1_{-1}) \cup (\tilde\eta^2_{-1})$, tangent to the line $y = c_1^*$ at the point $C_{-1} \in L_{-1}$, and a third arc $(\tilde\eta^3_{-1})$ belonging to $(\tilde\eta')$ (the preimage composed of period-two cycle points). An equivalent property takes place for the arc $(\tilde\eta')$ as well.

The stable manifold SSM of the slow dynamics consisting of the arcs of stable cycles can be visualized at small enough values of μ. As shown in Fig. 9 it is made of two subsets (red and black colored) related to each of the two parts of the cubic nonlinearity generating their own structure of the embedded boxes. This figure is obtained at $\mu = 10^{-6}$ by scanning y. The unstable manifold USM of the slow dynamics consisting of infinitely many arcs of unstable cycles (at $\mu = 0$) inside the region (W), occupies the space between the red and black arcs. One can recognize the points corresponding to the period-doubling at $\mu = 0$, two snap back repeller bifurcation of this fixed point, and a few arcs of stable period-two, three and four cycles. Figure 9 shows also that the stable manifold of the slow dynamics has contacts with the critical curve $L \cup L'$. The unstable manifold of slow dynamics continues out of

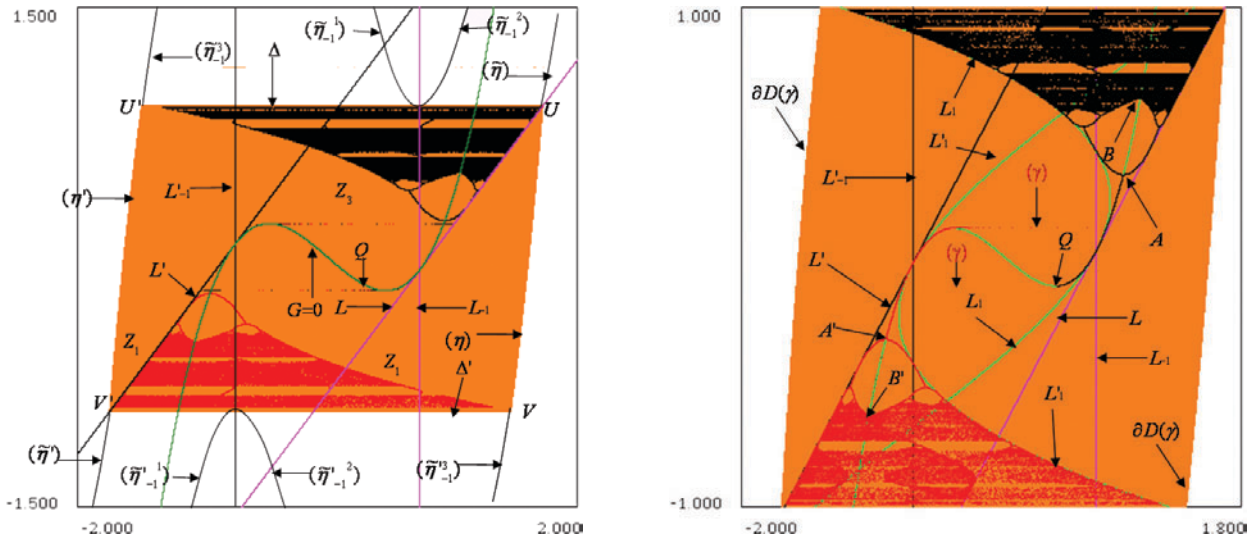

(a) (b)

Fig. 9. (a) Map (6) at $\mu = 10^{-6}$, $\alpha = 0.35$ and $d = 1.4$ showing the attractor SSM made of arcs of stable period-k cycles with multipliers $|S_2| < 1$. It is made up of two subsets (red and black) having the so-called embedded boxes structure, resides in domain (W) (orange) of nondiverging orbits bounded by two arcs $\widehat{U'V'}$ and $\widehat{UV}$ of unstable period-two cycles, and two horizontal segments $\overline{U'U}$ and $\overline{V'V}$. These arcs belong to the branches (η) and (η') consisting of unstable period-two cycles (ζ_1, ζ_2). The basin boundary ∂D contains the increasing rank preimages of the arcs $(\tilde\eta) = (\eta) \cap (y > c_1^*)$, $(\tilde\eta') = (\eta') \cap (y < c_1'^*)$. The figure also shows the rank-one preimages $(\tilde\eta_{-1}) = (\tilde\eta^1_{-1}) \cup (\tilde\eta^2_{-1}) \cup (\tilde\eta^3_{-1})$ of the arcs $(\tilde\eta)$ and $(\tilde\eta')$. The rank-one preimage $(\tilde\eta)_{-1} = T^{-1}(\tilde\eta)$ is formed by $(\tilde\eta_{-1}) = (\tilde\eta^1_{-1}) \cup (\tilde\eta^2_{-1})$, tangent to the line $y = c_1^*$ at the point $C_{-1} \in L_{-1}$, and a third arc $(\tilde\eta^3_{-1}) \in (\tilde\eta')$. (b) The map at $\mu = 10^{-5}$, $\alpha = -0.4$, $d = 0.45$ has an a stable invariant closed curve (γ). The stable manifold SSM is visualized by iterates of two close initial points (red and black) in $D(\gamma)$ transient toward (γ).

(W) below and above the segments $\overline{U'U}$ and $\overline{V'V}$ of ∂D.

5.4. *Dynamics of cubic map at* $0 < \mu \ll 1$

In the limit $\mu \to 0^+$, the arc Ψ_r of the nullcline $G = 0$ repels the fast motion if $(\partial G/\partial x) > 0$, i.e. when $d - 3x^2 > 0$. A necessary condition that an arc Ψ_a^i of $G = 0$ $(i = 1, 2)$ attracts the fast motion is $(\partial G/\partial x) < 0$. The arc Ψ_r is composed of unstable fixed points with fast multipliers $S_2 > 1$ at $\mu = 0$. The two arcs Ψ_r^i, $i = 1, 2$ are composed of fixed points with multiplier S_2 such that $S_2 < -1$ at $\mu = 0$. At $0 < \mu \ll 1$, the slow dynamics manifold originates from the Lattes' critical case (Sec. 3.2). Suppose that the map has an attracting set, like a stable invariant closed curve (γ) shown in Fig. 9 at $\alpha = -0.4$, $d = 0.45$ and $\mu = 10^{-5}$. The stable manifold SSM of the slow dynamics associated with this set can be easily visualized by iterations of two initial points inside the basin $D(\gamma)$ close to the horizontal parts of its boundary. When μ is sufficiently small, the manifold SSM shown in Fig. 9 by the red and black arcs, represents the transient toward the stable invariant closed curve (γ), which consists of two horizontal arcs of fast dynamics and two arcs of slow dynamics belonging to Ψ_a^i $(i = 1, 2)$. The manifolds of slow dynamics are now invariant curves of T^k, $k = 1, 2, 3, \ldots$, issued off perturbations of the "germ" $SM_{\mu=0}$. The perturbation of the unstable manifold USM_i belonging to the slow dynamics USM inside the region (W) is formed by infinitely many arcs occupying places (not visible at the figure scale, except for low period cycles) between the red and black arcs. Figure 9 does not permit to see the perturbation of the "germinal" unstable "slow" manifold USM_o outside of (W). At $0 < \mu \ll 1$, $y > c_1^*$, or $y < c_1'^*$ the basin boundary $\partial D(\gamma)$ results from this "germ" USM_o defined at $\mu = 0$. In this region a section $y = c$ gives a Cantor set of disjoint points, boundary of infinitely many open segments belonging to the basin $D(\gamma)$. The form of the basin boundary $\partial D(\gamma)$ is seen clearly at larger values of μ, as, for example, in Fig. 10(a). The picture indicates that $\partial D(Q)$ should have points on $y = \pm\infty$. As in the quadratic case, the bifurcation of a period-k arc USM_0 generates an unstable period-k cycle located on the boundary of the attracting set.

For small values of $|\mu|$, a plethora of attracting sets of the map can be observed by integration of the perturbation of a part of SSM into the attracting set itself. So, Fig. 10(b) represents a chaotic area (d) and the transient toward this attracting set. In Fig. 11(a), the attracting set is made up of two different chaotic areas (d) and (d'), whose basins are shown in green and yellow colors. Figure 11(b)

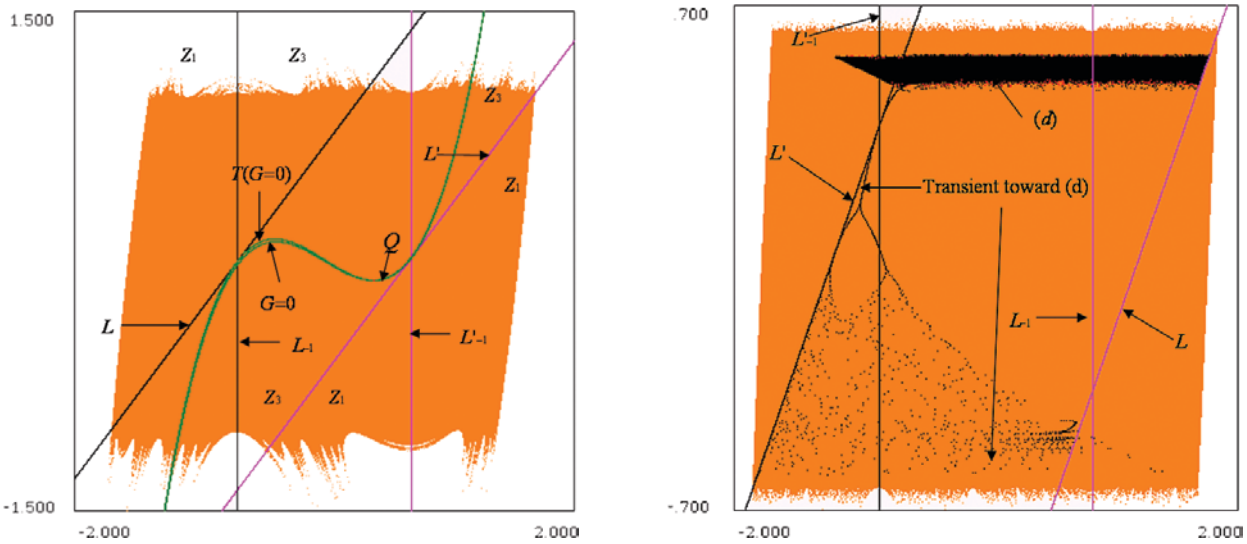

(a) (b)

Fig. 10. (a) Map (6), at $\mu = 0.02$, $\alpha = -0.4$ and $d = 0.45$, has the stable fixed point Q. Here, the bifurcation of the arcs of USM_0 determine the basin boundary $\partial D(Q)$. (b) Map (6) at $\mu = 0.001$, $\alpha = -0.2$, $d = 1.15$, possesses a chaotic area (d) and the transient toward the attracting set.

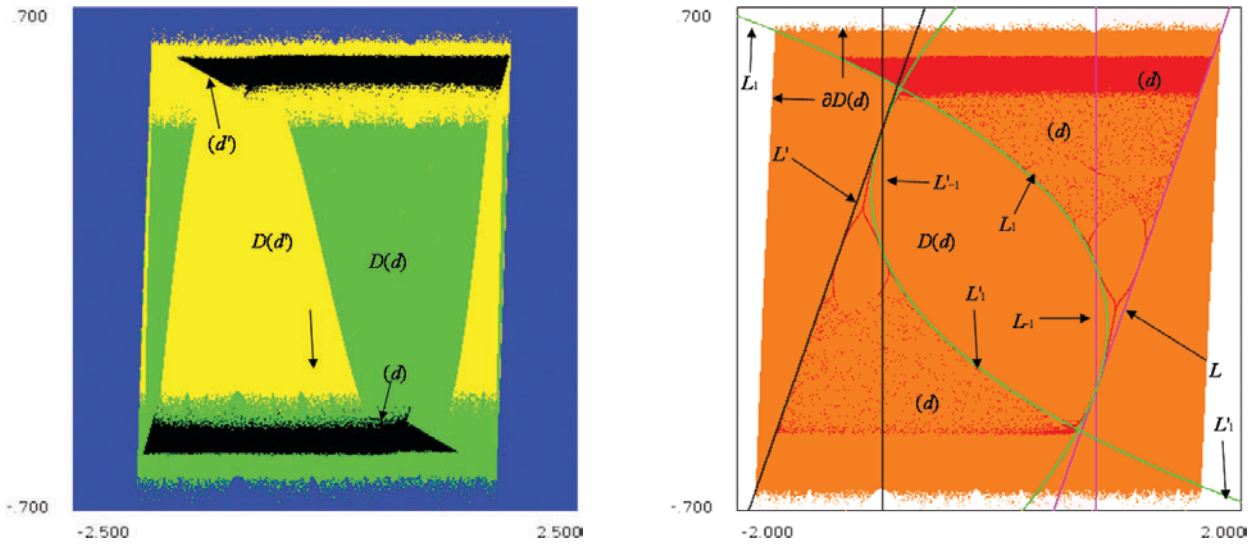

(a) (b)

Fig. 11. (a) Map (6), at $\mu = 0.0015$, $\alpha = -0.1$, $d = 1.2$ after an integration of the perturbed SSM into an attracting set consisting of two different chaotic areas (d) and (d'); their basins are colored green and yellow. (b) Map (6), at $\mu = 0.001$, $\alpha = -0.2$, $d = 1.145$, has a single chaotic area (d) after the merging of two chaotic areas.

demonstrates the united chaotic area (d) after the above chaotic areas have merged. Three insets in Fig. 12 represent the different looks of the chaotic areas found by integrating parts of SSM_0 converging to a stable invariant curve. With μ small enough and the fixed point Q on the repelling arc Ψ_r, a large diversity of attractors can be detected by fitting the ordinates of the $G = 0$ extrema (located at $x_e = \pm\sqrt{d/3}$, $y_e = \mp(2/3)\sqrt{d/3}$) to a bifurcation value producing fast dynamics for (7) on the cut $c = y_e$.

5.5. *Stable invariant sets*

5.5.1. *Invariant close curves*

A stable invariant close curve (γ) with a basin $D(\gamma)$, emerges at $\mu + d = 3\alpha^2$ when the stable $(\mu > (d - 3\alpha^2)^2/4,\ \mu + d < 3\alpha^2)$ focus fixed point $Q(-\alpha; \alpha^3 + \alpha)$ becomes unstable for $\mu + d > 3\alpha^2$. This occurs in an $O(\mu)$-neighborhood of the minimum $(\sqrt{d/3},\ -2\sqrt{d/3}/3)$ of the nullcline $G = 0$, which is a necessary condition for a canard birth. Figure 13 illustrates a situation similar to that for quadratic maps depicted in Fig. 3, where an arc of (γ) stays $O(\mu^a)$-close $(0 < a < 1)$ to the repelling arc Ψ_r of $G = 0$ in the limit $\mu \to 0^+$. The local behavior of (γ) is typical, until it does not cross the coincident preimages lines L_{-1} and L'_{-1}, i.e. until it has no contact with the critical lines L and L'. If it does, the noninvertibility feature of the map steps into action. Note that the intersection point $M \in (\gamma) \cap (G = 0)$ implies a vertical tangency between M and $M' \in T(G = 0)$. The curve (γ) crossing only one of the two attracting arcs Ψ_a^2 of $G = 0$, and the repelling arc Ψ_r is referred to *as* "*small*" invariant closed curve in Fig. 13.

As α is increased from $\alpha = -0.4$ to -0.38 ($\mu = 0.1$ and $d = 0.45$ are fixed), the size of (γ) increases too, so that it crosses $LC_{-1} = L_{-1} \cup L'_{-1}$, see Fig. 13(b). Its tangential contacts with the critical lines L and L' cause oscillations on (γ) [cf. Fig. 1(a)]. At $\alpha = -0.4$ and $d = 0.53$, (γ) starts to self-intersect, and losing smoothness it turns into a weakly chaotic ring $(\tilde{\gamma})$ shown in Fig. 14.

Let us consider next smaller values of μ, and start from the point ($\mu = 0.001$; $\alpha = -0.36509014$; $d = 0.4$) giving a small stable invariant closed curve (γ) in Fig. 13(a); observe that the minimum of $G = 0$ is in the interior of (γ). Dependence of (γ) on α is enormous; its size increases quickly with small variations of α. So, at $\mu = 0.001$, $\alpha = -0.36509$ and $d = 0.4$, the invariant curve (γ) ceases to be "small", and turns into a "duck" solution, depicted in Fig. 14(b). At some intermediate α, the fast component of (γ) becomes fuzzy, as reflected in Fig. 15(a).

A small increase to $\alpha = -0.36509013737915$ extends a fuzzy region joining now the "small" invariant curve with the "duck" one, like shown

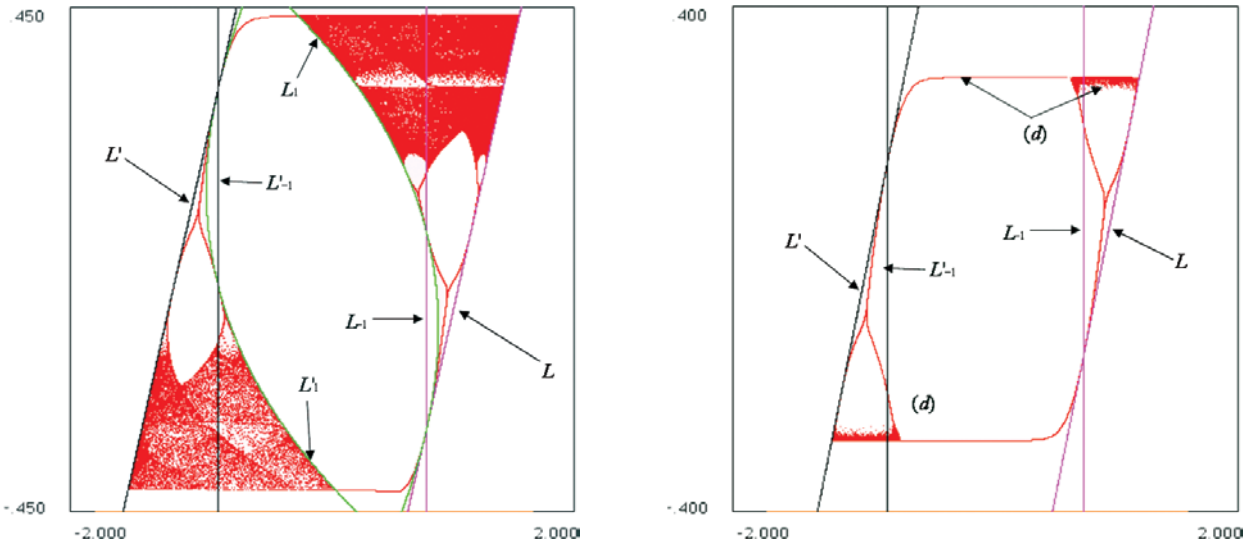

Fig. 12. Phase portraits of map (6) at (a) $\mu = 0.001$, $\alpha = -0.59$, $d = 1.05$; (b) $\alpha = 0.01$, $d = 0.8$; (c) $\alpha = 0.1$, $d = 0.9$, show iterates of the initial stable manifold SSM at $\mu = 0$ of slow dynamics converging to a stable invariant closed curve.

in Fig. 15(b). For $\alpha = -0.365090137379148$, the attractor is a canard type, with a single fuzzy fast component (Fig. 16). Likewise the quadratic map, due to computer roundups and truncation, the quantitative description of transformations of the attracting sets of the map, including the exact values for α corresponding to Figs. 15 and 16, are meaningless if depending on the computational platform arithmetic. So, an evolution of "small" invariant closed curve into the "duck" solution must be understood in a qualitative way with a certain scepticism regarding the mathematical rigor about the "fuzzy" arcs.

Figures 17(a) and 17(b) illustrate the stable invariant close curve (γ) consisting of two arcs of fast motion and two arcs of slow motion in a neighborhood of two attracting branches Ψ_a^i of the nullcline $G = 0$. When the curve (γ) starts intersecting L_{-1}, the oscillations of (γ) emerge, which are due to a contact with $L = T(L_{-1})$.

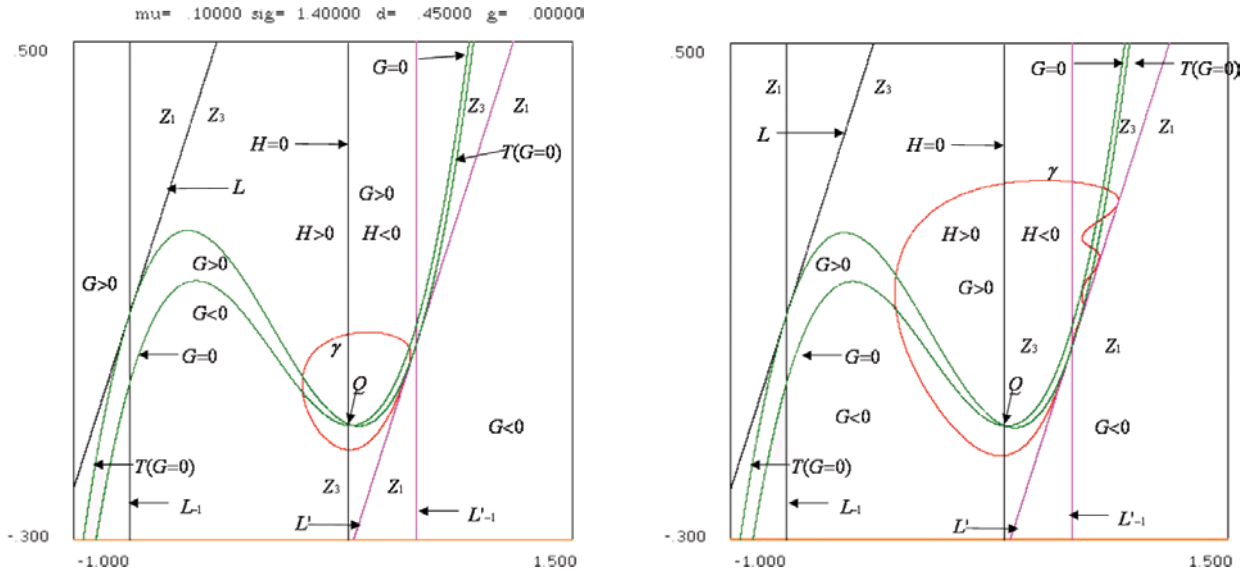

(a) (b)

Fig. 13. (a) Map (6), at $\mu = 0.1$, $\alpha = -0.4$, $d = 0.45$, depicts a circle (γ) not crossing the lines of preimages L_{-1} and L'_{-1}, and thus having no contact with critical lines L, L'. (b) Map (6), at $\mu = 0.1$, $\alpha = -0.38$, $d = 0.45$. Increasing the size of (γ) leads to its intersections with $LC_{-1} = L_{-1} \cup L'_{-1}$ and cause wiggles of (γ).

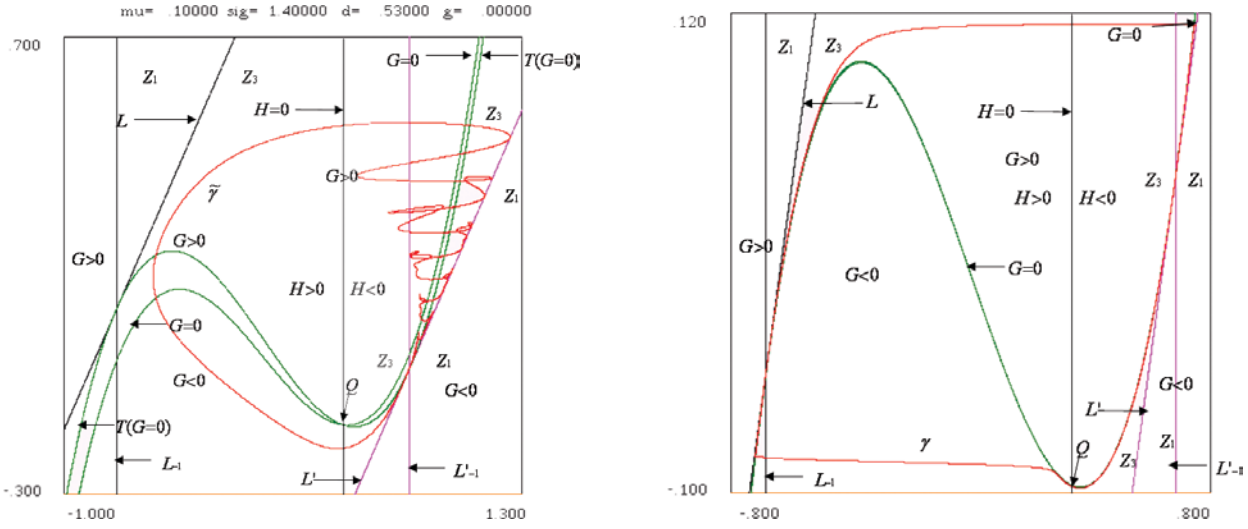

(a) (b)

Fig. 14. (a) Map at $\mu = 0.1$, $\alpha = -0.4$, $d = 0.53$, self-intersections of (γ) [compare with Fig. 1(c)] turn it into a weakly chaotic ring ($\tilde{\gamma}$). (b) At $\mu = 0.001$, $\alpha = -0.36509$, $d = 0.4$, the small appendix on (γ) follows the right knee of $G = 0$ including the unstable branch thereby creating the "duck with a head" configuration.

5.5.2. *Noninvertibility effect on the attractor and its basin*

A chaotic attractor (d) and its basin $\partial D(d)$ of a genuine noninvertible map may be in a way more complex. A first example is given in Fig. 18, where the chaotic area (d) is bounded by arcs of $LC = L \cup L'$ and their images $LC_n = L_n \cup L'_n$, $n = 1, 2, \ldots$, $LC_n = T^n(LC)$. Its enlargement shows the "spindly" fragment of (d) resembling the mechanism of self-intersections suggested in Fig. 1(c). An increase of the parameter $d = 0.8923$ leads to the situation, depicted in Fig. 19(a), occurring nearby the bifurcation destroying the attractor (d) when its boundary approaches the boundary $\partial D(d)$ of its

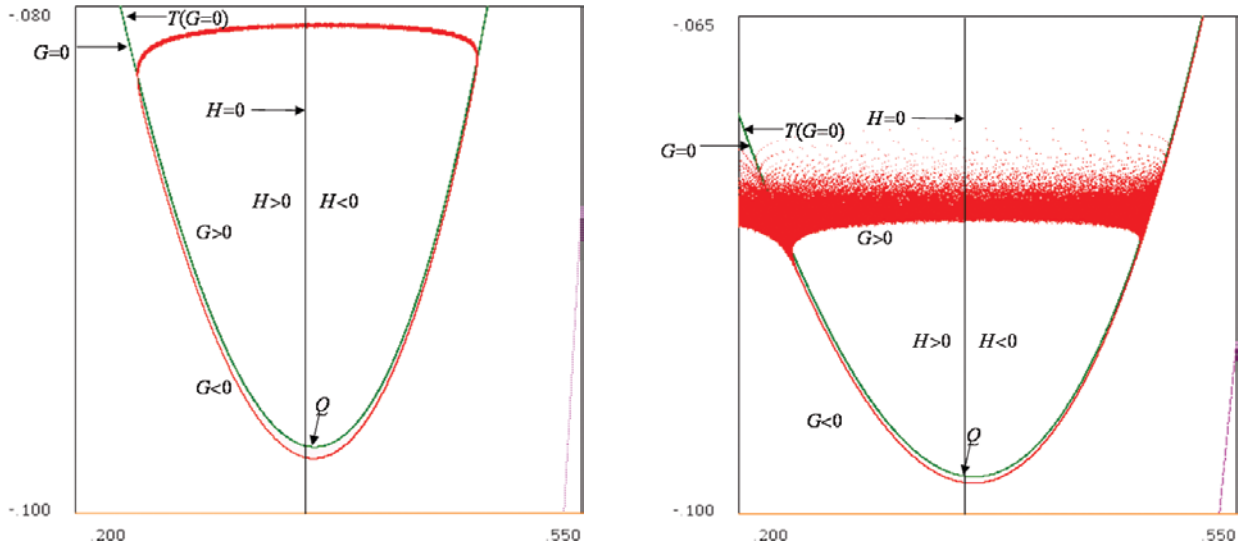

(a) (b)

Fig. 15. (a) Map (6), at $\mu = 0.001$, $\alpha = -0.36509013737916$, $d = 0.4$, seems to exhibit a "small invariant closed curve" (γ); indeed that attractor has a fractal structure; its horizontal segment disintegrates and becomes fuzzy. This fast component is zoomed in the next figure at $\alpha = -0.36509013737915$.

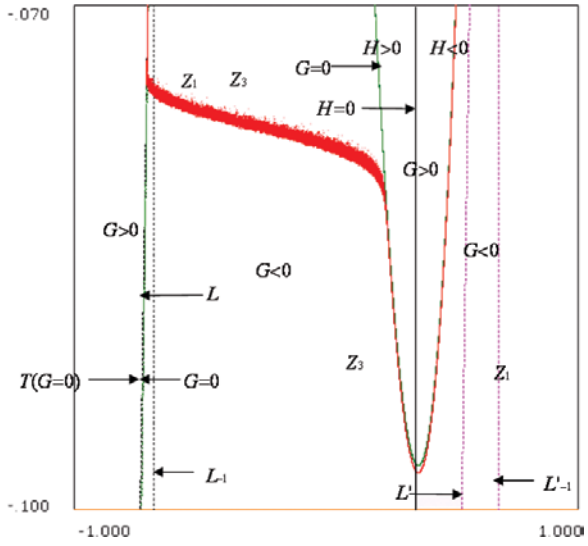

Fig. 16. (a) Cubic map (6), at $\mu = 0.001$, $\alpha = -0.365090137379148$, $d = 0.4$, has a canard-type attractor with one fuzzy fast motion component.

basin $D(d)$. This basin is multiply connected due to the presence of two bays H_0 and H_0' leading to two arborescent sequences of lakes with increasing rank preimages of H_0 and H_0', see the first preimages $T^{-1}(H_0) = H_1^1 \cup H_1^2 \cup H_1^3$ and $T^{-1}(H_0') = H_1'^1 \cup H_1'^2 \cup H_1'^3$ in Figs. 29(a) and 30.

A second example presented in Fig. 19(b) shows the attractor whose basin is nonconnected. Here, the attractor is a small invariant closed curve (γ) composed of the one arc of fast motion, and two arcs of slow motions: one in a Ψ_r neighborhood of $G = 0$, and the other near Ψ_a. A third example illustrating a dynamical variety is Fig. 20(a) at $\mu = 0.001$, $\alpha = -0.591681$, $d = 1.05$; the enlargement in Fig. 20(b) reveals the canard effect.

5.5.3. *From "small" invariant closed curve to canard*

Take note that the "small" invariant closed curve (γ) and the canard closed curve are related: an arc of (γ) remains in a small neighborhood of a piece of the repelling arc Ψ_r of the nullcline $G = 0$. Such a case is "exceptional" in the sense that it occurs within an extremely thin region in the parameter space. As mentioned above, the corresponding necessary condition is the following: the fixed point $Q(-\alpha; \alpha(\alpha^2 - d))$ is an unstable focus (when $\mu > (d - 3\alpha^2)^2/4$, $\mu + d > 3\alpha^2$), located in a small enough neighborhood of an extremum ($x = x_e = \pm\sqrt{d/3}$, $y = \mp(2/3)\sqrt{d/3}$) of the nullcline $G = 0$, i.e. the value of the parameter α must be rather close to $\mp\sqrt{d/3}$. The emerging "small" curve (γ) exists when it intersects the repelling arc Ψ_r of $G = 0$, which is not the case for the canard curve. A "large" invariant closed curve emerges when (γ) not only does not intersect Ψ_r, but also it has no arc staying inside a small neighborhood of a piece of the

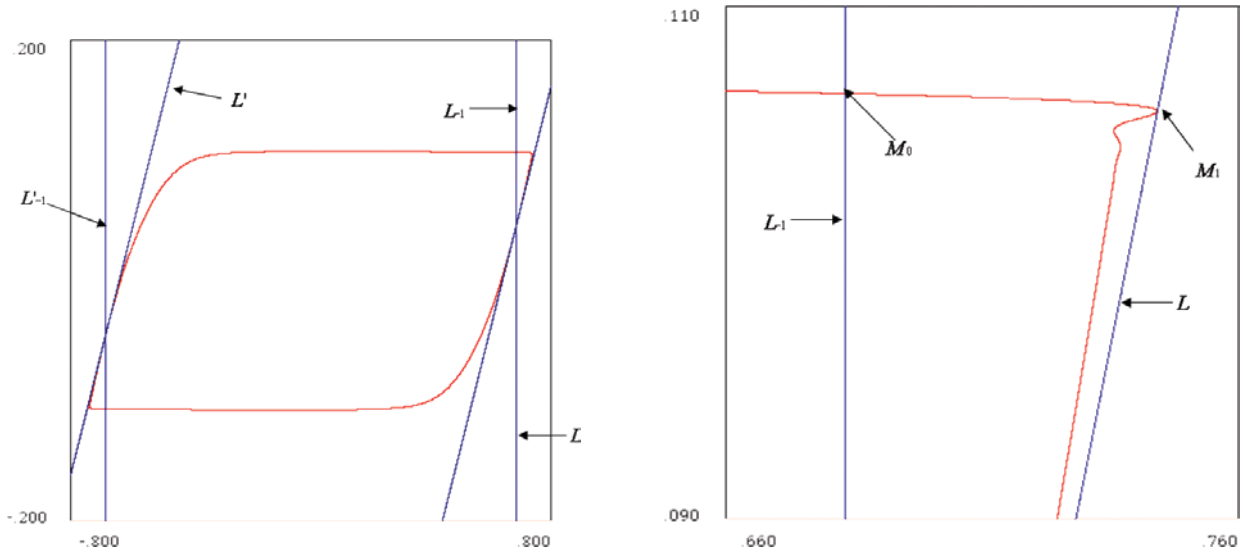

(a) (b)

Fig. 17. Map (6), at $\mu = 0.001$, $\alpha = 0$, $d = 0.4$, shows the classical situation where (a) the stable invariant close curve (γ) is composed of a pair of fast motion arcs, and those of slow motion near the attracting branches Ψ_a of $G = 0$; (b) Enlargement shows the intersection of (γ) with $LC_{-1} = L_{-1} \cup L'_{-1}$ leading to wiggles of (γ) due to its contact with $LC = L \cup L'$; (γ) is tangent to L at the point $T(M_0) = M_1$ and $M_0 = (\gamma) \cap L_{-1}$.

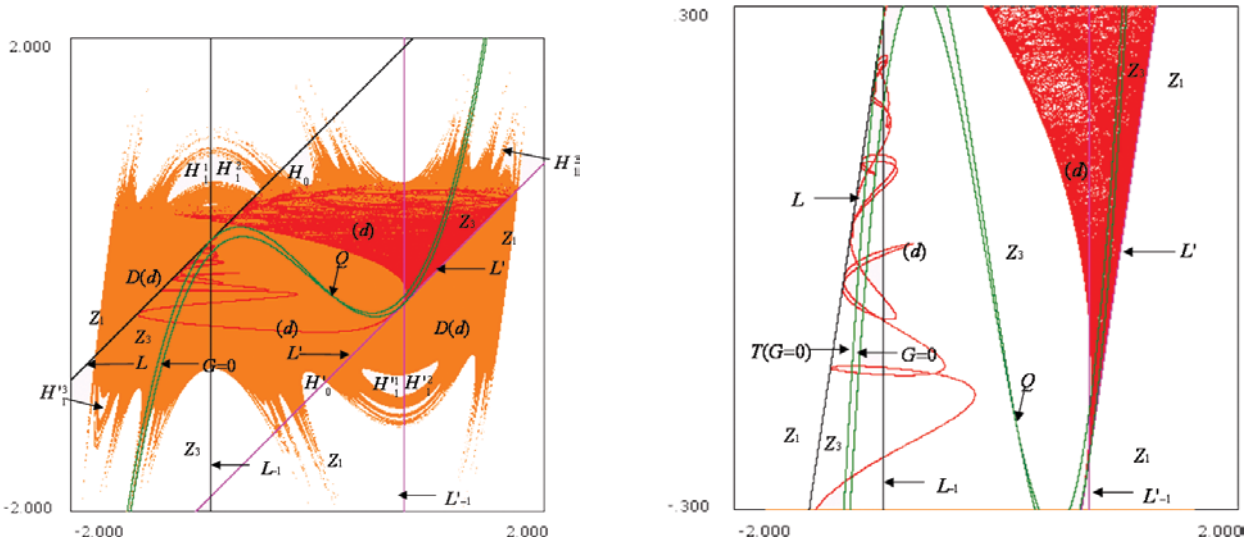

(a) (b)

Fig. 18. (a) Chaotic attractor (d) at $\mu = 0.1$, $\alpha = -0.25$, $d = 0.89$. (b) Enlargement showing that the spindly part of (d) corresponds to the scenario suggested in Fig. 1(c).

arc Ψ_r. Recall that Ψ_r repels the fast motion if $(\partial G/\partial x) > 0$, i.e. $d - 3x^2 > 0$ when $\mu \to 0^+$, i.e. the "repelling" action of Ψ_r is enforced starting from each of the two extrema up to the inflexion point $(x = y = 0)$ of $G = 0$, where it reaches the maximum $G_x = d$ (Ψ_r slope equals $-d$).

The parameter values corresponding to phase portraits in Figs. 15 and 16, yield a first type of transition from a "small" invariant closed curve (γ) to a canard. The transition is characterized by a sudden discontinuous change of the size of (γ) occurring at rather very small variations of a control parameter, other than $0 < \mu \ll 1$ surely. When μ is not small, a second type of transition occurs, characterized by the change of size of (γ) continuous with respect to control parameter variations.

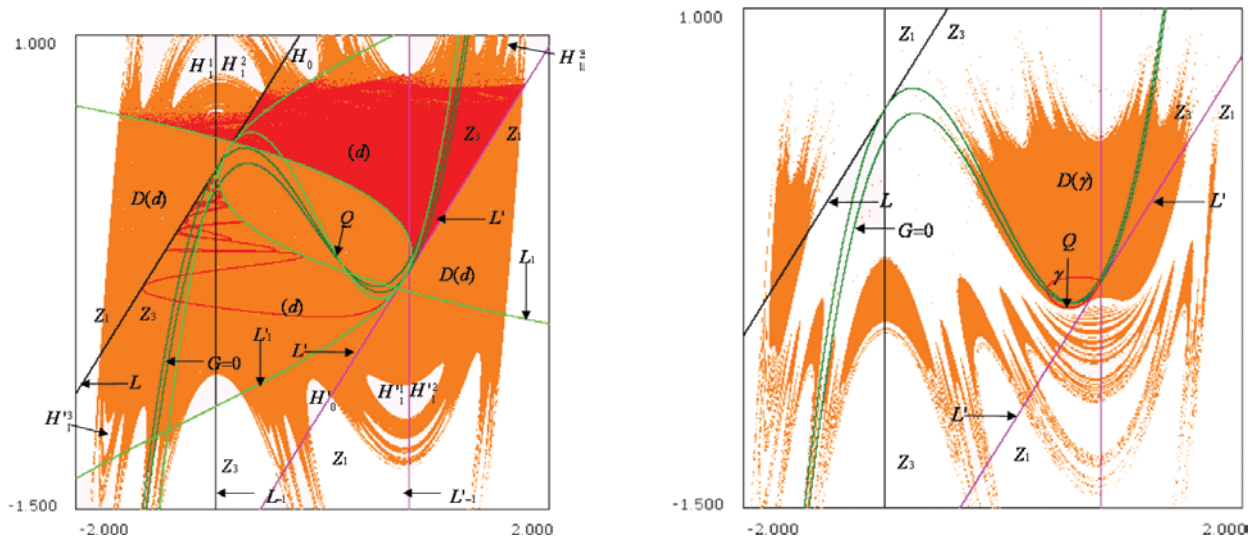

(a) (b)

Fig. 19. (a) Map (6), at $\mu = 0.1$, $\alpha = -0.25$, $d = 0.8923$ near the bifurcation destroying the attractor (d), when its boundary approaches $\partial D(d)$ of the multiply connected basin $D(d)$. (b) The attractor, which is a small invariant closed curve (γ) has disconnected basin at $\mu = 0.1$, $\alpha = -0.63$ and $d = 1.15$.

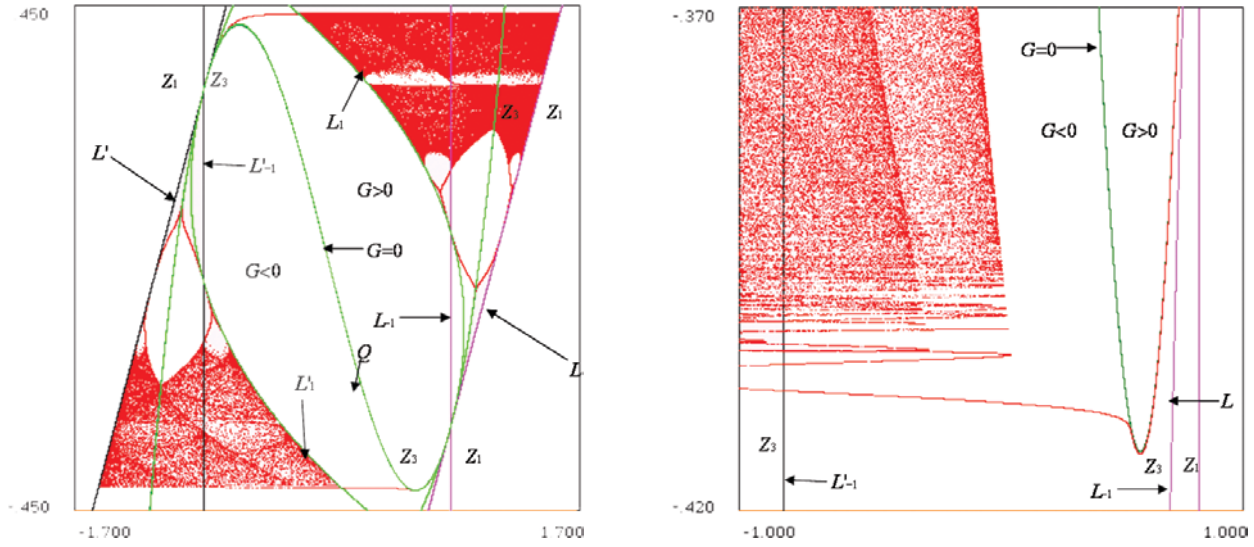

(a) (b)

Fig. 20. Map (6), $\mu = 0.001$, $\alpha = -0.591681$, $d = 1.05$ exhibits another type of chaotic attractor (a), whose enlargement (b) reveals the canard.

Figures 21(a)–21(e) show the transition of the second type with the continuous evolution of (γ) in the size, when α increases respectively from -0.37, through -0.3635, -0.3634, -0.3633 and -0.3628 at fixed $\mu = 0.02$ and $d = 0.4$. The stages of the transformation begins with the stable invariant closed curve (γ) bifurcating from Q in the neighborhood of the minimum ($x = \sqrt{d/3} \simeq 0.36515$, $y = -(2/3)\sqrt{d/3}$) of the nullcline $G = 0$.

After this bifurcation occurs at $\alpha_b \simeq -0.37417$, the fixed point Q is located on the arc Ψ_a^2 of $G = 0$ with a positive slope, where it stays until $x(Q) = -\sqrt{d/3} \simeq 0.36515$. When $\alpha > -\sqrt{d/3}$, the point Q moves onto the arc Ψ_r of $G = 0$ with a negative slope equal to $-\partial G/\partial x$, so that an arc of (γ) lies in a vicinity of Ψ_r. A necessary condition for the existence of a "small" curve (γ) becoming a canard is thus fulfilled. Let us elaborate on the

case, shown in Fig. 22, where (γ) emerges from Q in the neighborhood of the minimum $(x = \sqrt{d/3}$, $y = -(2/3)\sqrt{d/3})$ of the nullcline $G = 0$, thus $\alpha < 0$. The slope of the vector $\overrightarrow{MM'}$, connecting the image $M' = TM$ with its pre-image, is given by

$$\frac{\Delta y}{\Delta x} = \frac{y' - y}{x' - x} = \frac{-\mu(x + \alpha)}{G(x, y)}.$$

Following [Mishchenko & Pontryagin, 1955] and [Andronov *et al.*, 1959] for ODE, introduce the neighborhood $O(\mu^a)$ $(0 < a < 1)$ of the nullcline $G = 0$ that shrinks to $G = 0$ as $\mu \to 0^+$. Let B, $x(B) = x_m$, be the point on (γ) such that its forward image $B' = T(B)$ belongs to $G = 0$, and let A be the point on (γ) with the ordinate corresponding to the minimum of $G = 0$. Take note that between the points B' and $T(B')$ on (γ), there is a point leading to a vertical tangency (cf. Sec. 5.5.1), so that x_m is close to the smallest value of the abscissa of (γ). Let the function $G(x, y)$ be evaluated as $G(x, y) = -k(x)\mu^a$, $k(x) > 0$ along the arc $\widehat{AB}$ (of slow dynamics) of (γ), in the $O(\mu^a)$-neighborhood of the nullcline $G = 0$. Then, along $\widehat{AB}$, one has that $\Delta y/\Delta x = (x + \alpha)/[k(x)\mu^{a-1}]$, with $(x + \alpha) < 0$. Moreover, $|\Delta y|$ and $|\Delta x|$ are small since μ is small, and therefore $\Delta y/\Delta x$ is close to the slope of the line tangent to (γ). Pick a point (x^*, y^*) on the curve $G = 0$. Between its two extrema, the slope of $G(x^*, y^*) = 0$ is negative: $dy^*/dx^* = 3x^{*2} - d = -p(x^*)$, $p(x^*) > 0$. Note that $p(x^*)$ decreases from d to zero when x^* varies from zero to the minimum $x^* = \sqrt{d/3}$. Let (x, y) be a point on (γ) such that $y = y^*$. The condition of existence of a small invariant curve (γ) is that $\Delta y/\Delta x \le dy^*/dx^*$ along the arc $\widehat{AB}$ of (γ). This leads to the inequality:

$$\frac{\Delta y}{\Delta x} = \frac{x + \alpha}{k(x)\mu^{a-1}} \le -p(x^*), \quad \text{i.e. } -(x + \alpha) \ge \frac{p(x^*)k(x)}{\mu^{1-a}}, \tag{10}$$

where $-(x + \alpha) > 0$ is bounded, so that "small" curve (γ) must intersect $G = 0$ between its two extrema $(dy^*/dx^* < 0)$, i.e. $0 < -(x+\alpha) < 2\sqrt{d/3}$. So, inequality (10) is only fulfilled within a very narrow window of the parameter values. With $y = y^*$, decreasing x means increasing $-(x + \alpha)$ and $p(x^*)$, and hence (γ)'s size is increasing as well. The larger the values of μ, or α are chosen, the more the size of the "small" curve (γ) can grow. For example, at $x^* = 0$ $(p(x^*) = d)$, for the existence of (γ) it is required that $\sqrt{d/3} - k(x)\mu^a \ge k(x)d/\mu^{1-a}$, i.e. μ must be sufficiently large. Increasing $\alpha < 0$ ensures a fulfilment of the continuous growth of (γ) with no turning into the canard because $p(x^*)$ decreases from d $(x^* = 0)$ to 0 $(x^* = -\sqrt{d/3}$, which is the maximum on the nullcline $G = 0)$. Let us note that, with no μ large enough, (γ) cannot have a point $x = 0$ for which at the limit

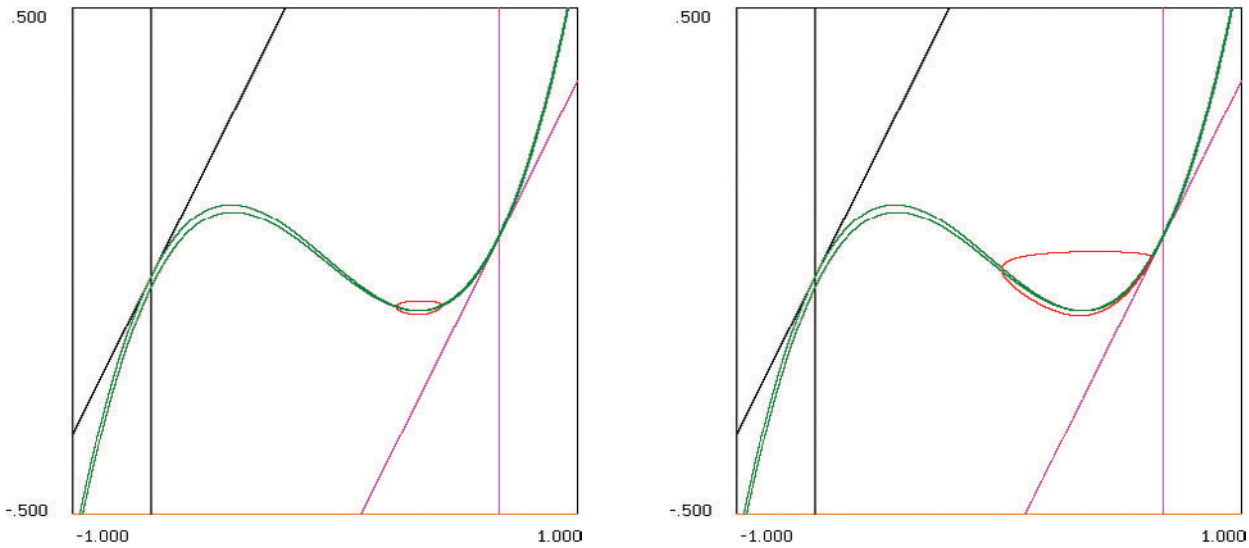

(a) (b)

Fig. 21. Stages of the evolution of a canard in map (6), at fixed $\mu = 0.02$, $d = 0.4$, as α increases from (a) -0.37, (b) 0.3635, (c) -0.3634, (d) -0.3633, through (e) -0.3628.

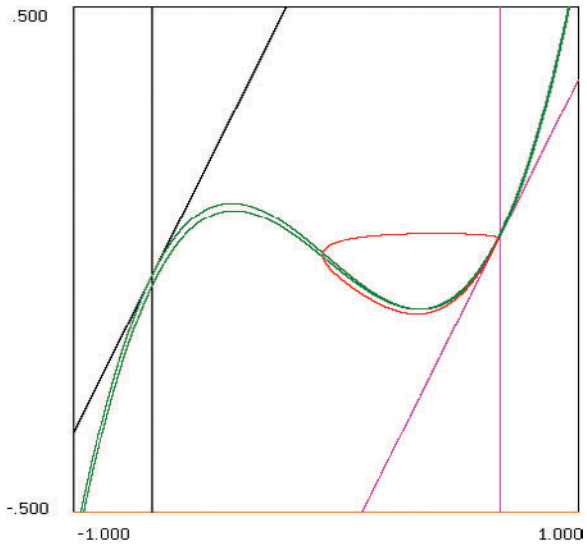

(c)

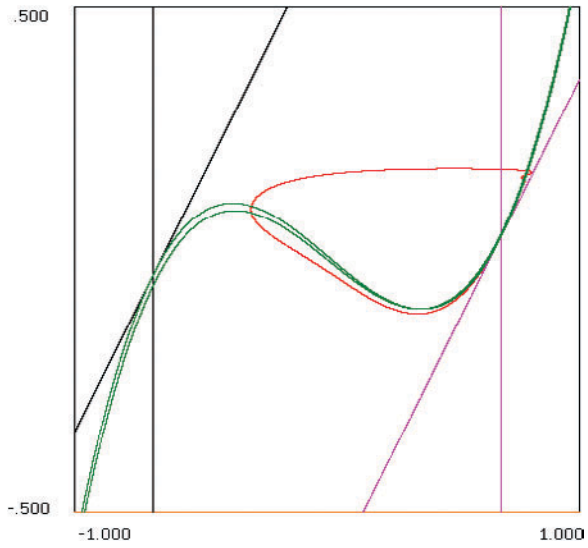

(d)

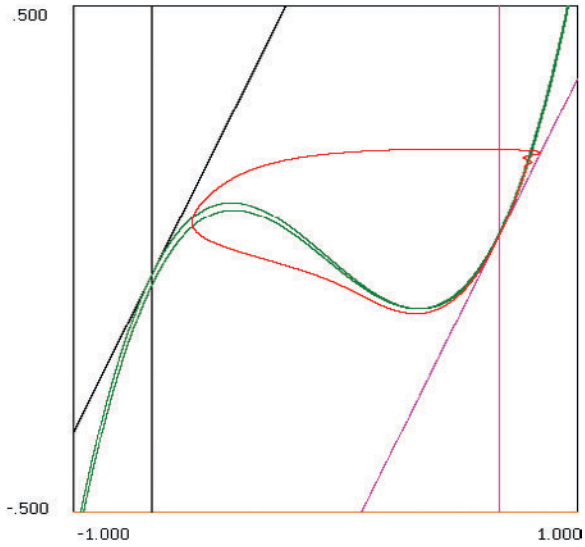

(e)

Fig. 21. (*Continued*)

$\sqrt{d/3} - k(x)\ \mu^a \geq k(x)d/\mu^{1-a}$. Then a continuous growth of the "small" invariant closed curve (γ) is impossible. As soon as (γ) has a point $x = 0$, an increase of the (γ) size cannot lead to a canard, because $|p(x^*)|$ decreases.

In the inequality (10) the ratio $p(x^*)/\mu^{1-a}$ plays a more important role. When $|\mu| \ll 1$, $p(x^*)$ must remain of order μ^{1-a} for the persistence of small (γ). Its sudden switch into the canard begins when (γ) has a point (x, y) satisfying the "inverse" inequality $-(x+\alpha) < p(x^*)k(x)/\mu^{1-a}$, i.e. $\Delta y/\Delta x < dy^*/dx^*$, $y(x) = y(x^*)$. Provided $p(x^*)$ is not sufficiently small and μ is not large enough, an orbit, having followed a small arc of Ψ_r in the $O(\mu^a)$-neighborhood of $G = 0$, from its minimum $p(x_e^*) = 0$ (where (10) is held), will be expelled from $O(\mu^a)$ by Ψ_r in a direction determined by the fast motion, i.e. the x-coordinate starts decreasing quickly. This leads to a formation of a new canard-like closed curve (γ).

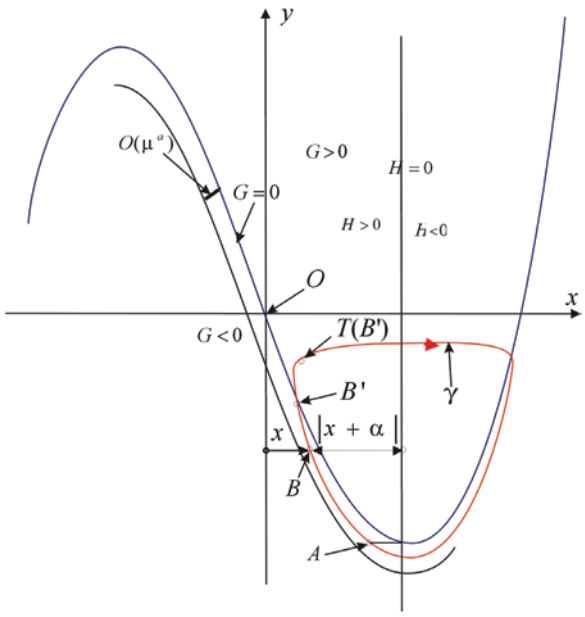

Fig. 22. Qualitative representation of the small stable invariant closed curve (γ) emerging from the fixed point Q residing nearby the minimum $(\sqrt{d/3}, -(2/3)\sqrt{d/3})$ of null-cline $G = 0$.

6. Conclusion

This paper is based on the important observation that a noninvertible two-dimensional degenerated map in the form $x' = x + G(x, y)$, $y' = y$ can be embedded into the family of the singularly perturbed maps $x' = x + G(x, y)$, $y' = y - \mu(x + \alpha)$, with $|\mu| \ll 1$. Indeed, when $\mu = 0$, an initial condition $y = c$, $c \in R^1$, yields the fast motion equation defined by the one-dimensional noninvertible map $x' = x + G(x, c)$. The constant c plays the role of a parameter in the family quadratic map with $G \equiv c + x^2$, or in a cubic one when $G \equiv c + dx - x^3$, whose dynamics are well known. For the map $x' = x + G(x, y)$, $y' = y - \mu(x + \alpha)$, the limit case $\mu = 0$ corresponds to the *Lattes' critical case* [1906], associated with a bifurcation described in [Gumowski & Mira, 1980, pp. 175–177, 252–260], and the case of μ going through zero in [Mira, 1987, pp. 206–211]. In this critical case, the manifold SM of slow dynamics in the (x, y)-plane is formed by all the cycles, and their limit points, generated as c varies, i.e. by infinitely many arcs made up of cycle points and their limits. Each period-k cycle, denoted by $(k; j)$ (the index j differentiates two cycles having the same period but exchanging differently their points by k applications of the map), generates a set SM_k^j of k arcs. The stable (resp. unstable) slow dynamics manifold SSM (resp. USM) is composed of all the stable (resp. unstable) arcs SSM_k^j (resp. USM_k^j) and their limit sets. Each point of SSM_k^j, or USM_k^j, corresponds to a period-k cycle with one of the two multipliers $S_1 = +1$, the second, fast, multiplier, S_2 is found from the map $x' = x + G(x, c)$.

The bifurcation occurring while crossing through the Lattes' critical case, results in the destruction of each set of k-arcs, consisting of the points of a period-k cycle with $S_1 = +1$, which may give rise to a period-k (or $2k$) cycle, $k = 1, 2, \ldots$ It is worth noting that at small enough values of μ, the stable slow dynamics manifold SSM may reproduce the classic bifurcation diagram of the one-dimensional map obtained through scanning by the control parameter c. In this sense, the case $\mu = 0$ appears as the "germinal" situation giving rise to the dynamics generated when $\mu \neq 0$.

The situation related to what is known as a "canard" or "French duck" limit cycle in autonomous ODEs, also occurs in the map $x' = x + G(x, y)$, $y' = y - \mu(x + \alpha)$ as well: a stable invariant closed curve exists within a narrow window of parameter values. However, because of the noninvertibility of the map, it may become into a attractor of a complex shape, which can be chaotic as well. Similar to ODEs, the canard behavior can be explained without the standard analysis tool [Callot *et al.*, 1977; Diener, 1981], but by applying the classical qualitative methods of dynamical systems, as shown in Sec. 5.5.3.

This study can be extended to other forms of function $G(x, y)$. For example, the map with $G(x, y) = y + px + qx^3 + rx^5$ may already generate two invariant closed curves: stable and unstable, with a plethora of different complex behaviors. Another direction in this context is to consider x, y and μ as vectors, i.e. a map of a higher dimension with a few time scales. All these extensions pave the way for new studies.

Acknowledgments

This work has been performed under the auspices of CNR, Italy, and under the activity of the national research project "Modelli dinamici in economia e finanza: evoluzione, incertezza e previsioni", MURST, Italy. A. Shilnikov acknowledges the RFBR grants No. 02-01-00273 and No. 01-01-00975, B&B seed grants.

References

Andronov, A. A., Witt, A. A. & Kaïkin, C. E. [1959] "Theory of oscillations," (Fizmatgiz, Moscow) (in Russian).

Callot, J. L., Diener, F. & Diener, M. [1977] "Chasse au canard," Publication 14/P-07 of Institut de Recherche Mathématique Avancée (IRMA, Strasbourg).

Diener, M. [1981] "Canards et bifurcations," in *Mathematical Tools and Models for Control, Systems Analysis and Signal Processing*, Vol. 3, CNRS (Toulouse/Paris), pp. 289–313.

Fenichel, F. [1979] "Geometric singular perturbation theory for ordinary differential equations," *J. Diff. Eqs.* **31**, 53–98.

Frouzakis, C. E., Gardini, L., Kevrekidis, I. G., Millerioux, G. & Mira, C. [1997] "On some properties of invariant sets of two-dimensional noninvertible maps," *Int. J. Bifurcation and Chaos* **7**, 1167–1194.

Gumowski, I. & Mira, C. [1977] "Solutions chaotiques bornées d'une récurrence ou transformation ponctuelle du second ordre à inverse non unique," *Comptes Rendus Acad. Sc. Paris, Série A* **285**, 477–480.

Gumowski, I. & Mira, C. [1978] "Bifurcation déstabilisant une solution chaotique d'un endomorphisme du 2nd ordre," *Comptes Rendus Acad. Sc. Paris, Série A* **286**, 427–431.

Gumowski, I. & Mira, C. [1980] *Dynamique Chaotique. Transformations Ponctuelles. Transition Ordre-désordre* (Editions Cépadues, Toulouse).

Lattes, S. [1906] "Sur les équations fonstionnelles qui définissent une courbe, ou une surface, invariantepar une transformation," *Ann. di Matematica* **3**, 1–137.

Michshenko, E. F. & Pontryagin, L. S. [1955] "Periodic solutions close to discontinuous ones, generated by a system of differential equations," *Dokl. Akad. Nauk SSSR* **152**, 889–893 (in Russian).

Michshenko, E. F. & Rozov, N. K. [1975] *Differential Equations with Small Parameters and Relaxation Oscillations* (Nauka, Moscow) (in Russian).

Mira, C. [1975] "Accumulations de bifurcations et structures boîtes-emboîtées dans les récurrences et transformations ponctuelles," *Proc. 7th Int. Conf. Nonlinear Oscillations*, Berlin, September 1975 (Akademic Verlag, Berlin), Band I 2, pp. 81–93.

Mira, C. [1987] *Chaotic Dynamics. From the One-dimensional Endomorphism to the Two-dimensional Diffeomorphism* (World Scientific, Singapore).

Mira, C., Fournier-Prunaret, D., Gardini, L., Kawakami, H. Cathala, J. C. [1994] "Basin bifurcations of two-dimensional noninvertible maps: Fractalization of basins," *Int. J. Bifurcation and Chaos* **4**, 343–381.

Mira, C., Gardini, L., Barugola, A. & Cathala, J. C. [1996] *Chaotic Dynamics in Two-dimensional Noninvertible Maps*, World Scientific Series on Nonlinear Sciences, Series A, Vol. 20, 630 pp.

Mira, C. [2000] "Chaos and fractal properties induced by noninvertibility of models in the form of maps," *Chaos Solit. Fract.* **11**, 251–262.

Pontryagin, L. S. [1957] "Asymptotic behavior of solutions a system of differential equations with small parameter coefficient of high order derivative," *Izv. Akad. Nauk SSSR*, Math. Series, Vol. 21, pp. 605–635.

Shilnikov, A. L. & Rulkov, N. F. [2003] "Origin of chaos in a two-dimensional map modelling spiking-bursting neural activity," *Int. J. Bifurcation and Chaos* **13**, 3325–3340.

Shilnikov, A. L. & Rulkov, N. F. [2004] "Subthreshold oscillations in a map-based neuron model," *Phys. Lett.* **A328**, 177–184.

Tikhonov, A. N. [1952] "Systems of differential equations containing a small parameter multiplying the derivative," *Mat. Sb.* **31**, 575–586.

Copyright of International Journal of Bifurcation & Chaos is the property of World Scientific Publishing Company and its content may not be copied or emailed to multiple sites or posted to a listserv without the copyright holder's express written permission. However, users may print, download, or email articles for individual use.